

Experimental Sections

Chemicals and the synthesis of the catalysts

KOD (30% in D₂O) is purchased from ABCR; ethanol (99.5%) is purchased from Fluka; 1 M KOH standard solution is purchased from Merck KGaA. All other chemicals were purchased from Sigma-Aldrich. The electrolytes were prepared by using ultra-pure water (18.2 MΩ/cm).

Pretreatment of nickel foam (NF) The NF was first cleaned by sonicating in acetone for 30 mins to remove the organic impurities. Then the NF was dried and dipped in 15% HCl for 30 mins with sonication. The electrode was washed by ultra-pure water and dried in room temperature. Noted that the electrode should be used within two hours, else the surface generated nickel hydroxide would decrease the adsorption ability of the catalysts (FeOOH).

Synthesis of FeOOH-NiOOH^[1] A cleaned NF electrode was dipped in 10 mM FeCl₃ solution with stirring for 15 mins. After that, the electrode was directly dried in 75 °C oven over night. The FeOOH-NiOOH was formed during the drying period.

Synthesis of NiFe LDH (20% Fe) We used a method according to previous literature with modifications.^[2] Typically, Ni(NO₃)₂·6H₂O (2.0 mmol, 582 mg), Fe(NO₃)₃·9H₂O (0.5 mmol, 202 mg), NH₄F (10 mmol, 371 mg) and urea (25 mmol, 1.50 g) were dissolved in H₂O (40 ml) with vigorous stirring. The mixed solution was stirred for 30 mins and then transferred to a 50 mL Teflon-lined stainless steel autoclave. The autoclave was heated at 120 °C for 16 h. After cooling down to room temperature, the yellowish solid was washed by ultrapure water for 3 times and ethanol for 1 time, and then naturally dried on a watch glass. If no special indication, the NiFe LDH samples mentioned in SI and main-text have 20% Fe content.

Synthesis of NiFe LDH (10% Fe) The synthetic procedure is a bit different to that of 20% Fe samples. Typically, the 40 mL DI water was degassed for 1h, before dissolving Ni(NO₃)₂·6H₂O (2.25 mmol, 654 mg), FeSO₄·7H₂O (0.25 mmol, 70 mg), NH₄F (10 mmol, 371 mg) and urea (25 mmol, 1.50 g). The mixed solution was stirred for 30 mins under nitrogen. Then the solution was sealed in a 50 mL Teflon-lined stainless steel autoclave. The autoclave was heated at 120 °C for 16 h. After cooling down to room temperature, the green solid was washed by ultrapure water for 3 times and ethanol for 1 time, and then naturally dried on a watch glass. The color of the solid will turn to yellow in the air, while the electrochemical property is not influenced by this color change.

Synthesis of Ni hydroxide The bulk Ni hydroxide was synthesized through a hydrothermal method.^[3] 0.10 M of Ni(NO₃)₂·6H₂O and 0.15 M of urea were dissolved in 80 mL of deionized water that was already boiled to remove dissolved CO₂ in it. The mixed solution was sonicated for 30 mins to make it homogeneous. Then, the resulting solution was transferred to a 50 mL Teflon-lined stainless steel autoclave and heated at 190 °C for 48 h. The as-obtained green product was collected by centrifugation as it washed with ultrapure water for 3 times and ethanol for 1 time.

Synthesis of γ -FeOOH The material was synthesized according to previous literature with modifications.^[1] Typically, 20 mL of 0.02 M $\text{Fe}(\text{NO}_3)_3$ solution was sealed in a glass container, which was then maintained at 75 °C for 24 h. After centrifuging and washing with water for 3 times and ethanol for 1 time, yellowish-brown powder was obtained as γ -FeOOH.

Preparation of Fe-free KOH The Fe-free KOH was prepared for Operando Raman experiments of pure NF and pure Ni hydroxide (see below). The Fe impurities in normal KOH solutions can be removed by treating with high-purity $\text{Ni}(\text{OH})_2$.^[4] In a clean 50 mL polypropylene centrifuge tube, 2 g of $\text{Ni}(\text{NO}_3)_2 \cdot 6\text{H}_2\text{O}$ (99.99%) was dissolved in 5 mL of ultrapure water. 20 mL of 1 M KOH solution was added to give a $\text{Ni}(\text{OH})_2$ precipitate. The suspension was agitated and centrifuged, and the supernatant was decanted. The $\text{Ni}(\text{OH})_2$ precipitate was washed with ultrapure water for three times by centrifugation. The solid was dispersed in 10 mL of 1 M KOH by centrifugation, and the supernatant was decanted. This solid was used as the Fe-absorber. The normal KOH solutions could be cleaned by adding to this $\text{Ni}(\text{OH})_2$. The cleaning procedure involves dispersing $\text{Ni}(\text{OH})_2$ in the KOH solution, mechanically agitated over-night, followed by at least 3 h of resting.

Characterizations

Powder X-ray diffraction (PXRD) measurements were carried out on an X'Pert Philips diffractometer in Bragg-Brentano geometry with monochromatic $\text{CuK}\alpha$ radiation (0.1541 nm) and a fast Si-PIN multi-strip detector. The step size was 0.02 degree s^{-1} . Transmission electron microscopy (TEM) was performed on an FEI Talos instrument that operated at 200 kV high tension. Energy dispersed X-ray (EDX) mapping was used for determining the distribution of the elemental compositions. The images were collected in HAADF-STEM (High-angle annular dark-field scanning transmission electron microscopy) mode and the mapping was performed in ESpirit software. Samples for TEM were prepared by drop-drying the samples from their diluted ethanol suspensions onto carbon-coated copper grids. Suspension of FeOOH-NiOOH was collected by sonicating the electrode in ethanol for 1h. ICP-AES (Inductively coupled plasma – Atomic Emission Spectroscopy) results were obtained by a Nexlon 350 (Perkin Elmer) machine. All the samples were dissolved by ultra-pure nitric acid (65%, Merck KGaA) then diluted by 30 times.

Raman spectroscopic experiments were performed at a Raman spectroscopy (inVia confocal Raman microscope, Renishaw) with a 63x water immersion objective (Leica-Microsystems) for both operando and ex-situ analysis. A transparent Teflon film (0.001 in thickness, McMaster Carr) was applied to cover the lens of the objective in order to prevent direct contact with electrolyte. The wavelength of the laser excitation source was 532 nm with a laser power of ~ 0.5 mW at a grating of 1800 l mm^{-1} . Charge coupled device (CCD) detector was used to collect the scattered light from electrode surface. Prior to use, peak position of Raman spectrum was calibrated based on 520 ± 0.5 cm^{-1} peak of silicon. Each spectrum was recorded with a resolution of ~ 1 cm^{-1} by setting up the measurement condition such that 30 consecutive scans and exposure time of 2 sec to laser at a beam spot were applied. All Raman experiments were carried out with a custom-

made electrochemical cell in which a platinum wire and a custom-made double-junction Ag/AgCl served as counter and reference electrodes respectively. Prior to each experiment, the cell was dipped in an acid bath to remove all traces of metals and other dirt, and subsequently it was rinsed with acetone, alcohol and distilled water. For FeOOH-NiOOH samples, they were pressed with a hydraulic machine at 5 tons to make them flat and thin enough to fit the electrochemical Raman cell. For other powder-type samples (LDHs), the same catalyst ink as used in electrochemical measurements was drop-casted on a thin Au foil and then dried. The catalyst deposited Au was employed for subsequent operando Raman spectroscopy experiments.

Electrochemical test conditions

FeOOH-NiOOH (geometric area: 0.2-0.3 cm²) was directly used for electrochemical measurements. For NiFe LDH samples, the catalyst ink was prepared by mixing of 1 mL water, 0.25 mL isopropanol, 0.01 mL 5 wt% Nafion solution and 3 mg materials. The ink was sonicated for at least 2 h. Then 160 μL/cm² of the ink was uniformly loaded onto a carbon cloth electrode (CC, plasma treated, geometric area: 0.2-0.3 cm²). The electrodes were dried in a 75 °C oven for 30 mins before measurements.

All of the electrochemical measurements in this study were independently repeated for at least three times. The electrochemical measurements were performed in a three-electrode electrochemical cell, in which Pt wire and Ag/AgCl electrode (saturated KCl, E(Ag/AgCl) = 0.197 V vs. NHE, normal hydrogen electrode) were used as counter and reference electrode, respectively. The working electrode and reference electrode were separated with counter electrode by a glass frit. All potentials were reported versus the reversible hydrogen electrode (RHE) unless otherwise specified. Before measurements, all of the electrolyte were calibrated the point of 0 V versus RHE by standard hydrogen saturation calibration experiments. A glassy carbon electrode drop-casted by Pt/C was used as the working electrode. After bubbling with hydrogen for 30 mins, the electrode was subjected to linear scan voltammetry (LSV, scan rate: 2 mV/s), in which the current of both hydrogen evolution and hydrogen oxidation could be observed. The cross-point is 0 V vs. RHE. Based on Eq. S1, the pH values of various electrolytes can be measured. The solution was stirred by a magnetic stirring bar in all of the electrochemical measurements. The polarization curves were recorded by LSV, and the scan rate was 1 mV/s, with 95% IR correction. The data was collected from cathodic potential to anodic potential (forward scan). 3 LSV scans were obtained for each measurements and the third LSV was used for analysis. The first LSV was typically influenced by oxidative peak. The Tafel plots were derived from LSVs. To investigate redox peaks, the scan rate was set to 10 mV/s, with 90% IR correction. The activation process is performed from 1.20-1.53 V vs. RHE. The scan rate is 10 mV/s, with 90% IR correction. The TOFs were calculated by Eq. S2, where J is the anodic current density at certain overpotential, A is the geometrical surface area of the electrode, F is the Faraday constant (96485 C/mol), and m is the loadings of Fe (assumed to be active sites).

$$E(\text{RHE}) = E(\text{Ag}/\text{AgCl}) + 0.197 \text{ V} + 0.0592 \times \text{pH} \text{ V} \quad (\text{S1})$$

$$TOF = \frac{J \times A}{4 \times F \times m} \quad (S2)$$

Double-layer capacitance of the working electrode (C_{dl}) was measured to calculate and compare the normalized activity.^[5] The C_{dl} was calculated according to Eq. S3, where j_a and j_c are charging and discharging current densities and v is the scan rate.^[5] The potential range of the measurements is from 1.00 to 1.10 V vs. RHE, where no catalytic current and Ni redox peaks were observed. The difference of charging and discharging current densities at 1.05 V was used for calculation. The scan rates were from 10 to 200 mV/s (10, 20, 50, 100, 150, and 200 mV/s). Then the normalized performance was obtained by divide current density to C_{dl} (j/C_{dl}).

$$C_{dl} = \frac{|j_a - j_c|}{2v} \quad (S3)$$

Electrokinetic studies were performed in KOH with concentration from 0.5 M – 2 M. The 0.5 M and 0.75 M KOH were prepared by dilute 1 M KOH standard solution, while 1.5 M and 2 M KOH were prepared by further adding desired amount of KOH flakes in 1 M KOH standard solution. The LSVs of investigated electrodes were obtained sequentially in 0.5 M, 0.75 M, 1 M, 1.5 M and 2 M KOH. The Tafel plots were derived from LSVs and linear fitted, as $(\partial E / \partial j)_{pH}$. The relationship between the potential (vs. SHE, Standard Hydrogen Electrode) at a constant current and the concentration of hydroxyl ions ($(\partial E / \partial \log[OH^-])_j$) were obtained by calculating the potential at a constant current (10 mA/cm² for FeOOH-NiOOH; 1 mA/cm² for NiFe LDH) and $\log [OH^-]$, and then linear fitting. The potential is referred to Ag/AgCl reference electrode, which is equivalent to referring to SHE (by adding 0.197 V). The order dependence on the hydroxyl ions ($(\partial j / \partial \log[OH^-])_E$) in 0.5-2 M KOH can be determined according to Eq. S4. This parameter should not be directly read from LSVs since it is hard to ensure that in a certain potential, all the current densities are in Tafel region for KOH with different concentrations.

$$\left(\frac{\partial \log j}{\partial \log [OH^-]} \right)_E = - \frac{\left(\frac{\partial E}{\partial \log [OH^-]} \right)_j}{\left(\frac{\partial E}{\partial \log j} \right)_{pH}} \quad (S4)$$

Cation effect of each catalysts was investigated in 1 M KOH, 1 M NaOH and 1 M LiOH. The point of 0 V vs. RHE of each electrolyte was calibrated by standard hydrogen saturation calibration method (see experimental section above). Noted that the apparent pH value of KOH, NaOH, LiOH is different, despite the same concentration. The pH values are 13.7, 13.5, 13.1 for 1 M KOH, NaOH, LiOH, respectively. The LSVs of investigated electrodes were obtained sequentially in 1 M KOH, 1 M NaOH and 1 M LiOH.

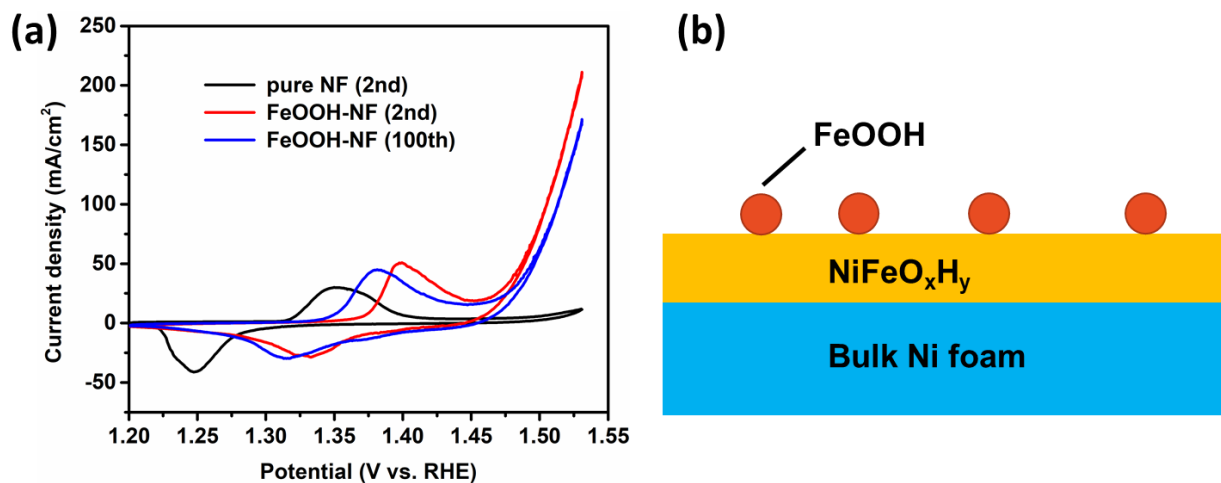
H/D isotope experiments were performed in 0.5 M and 1 M electrolyte. KOD in D₂O solution were prepared by diluting 30% KOD with D₂O to desired concentrations. The pH of KOH was calibrated by standard hydrogen saturation calibration method. The pD of KOD were calculated by adding 0.87 based on pH of KOH with same concentration. This treatment is according to the different pK_w values of H₂O (14.00) and D₂O (14.87). The isotope effect (IE) value is calculated by the ratio of the current density in KOH and KOD, in the same overpotential (Eq. S5). Noted that the

theoretical potential of OER in water is 1.229 V vs. RHE, while that of OER in D₂O is 1.262 V vs. RDE (reversible deuterium electrode).^[6] Therefore, the overpotential in KOH and in KOD is calculated as Eq. S6-S7.

$$IE = \frac{j_{KOH}}{j_{KOD}} \quad (S5)$$

$$\eta_{KOH} = E(Ag/AgCl) + 0.197 V + 0.0592 V \times pH - 1.229 V \quad (S6)$$

$$\eta_{KOD} = E(Ag/AgCl) + 0.197 V + 0.0592 V \times (pH + 0.87) - 1.262 V \quad (S7)$$



(c)

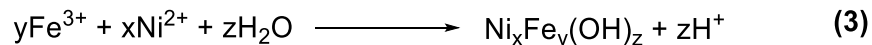
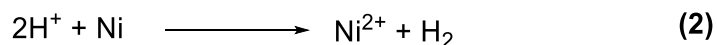
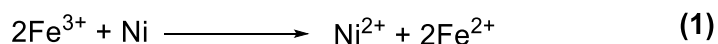


Figure S1 (a) 2nd (red) and 100th (blue) CVs of as-prepared FeOOH-NiOOH and 2nd of pure NF (black). (b) Illustrated scheme for the composition of FeOOH-NiOOH. (c) Possible reactions for generating Ni_xFe_y(OH)_z and FeOOH. Since the precursor Fe³⁺ solution is oxidative and acidic, Ni²⁺ is generated when dipping NF in Fe³⁺ solution.^[7] Then the Fe doped NiO_xH_y (NiFeO_xH_y, or Ni_xFe_y(OH)_z) is formed on the surface of NF during the drying process. The excess Fe is transformed to iron oxyhydroxides (FeOOH) after drying. The 2nd CV was adopted since the 1st CV contains big background signals.

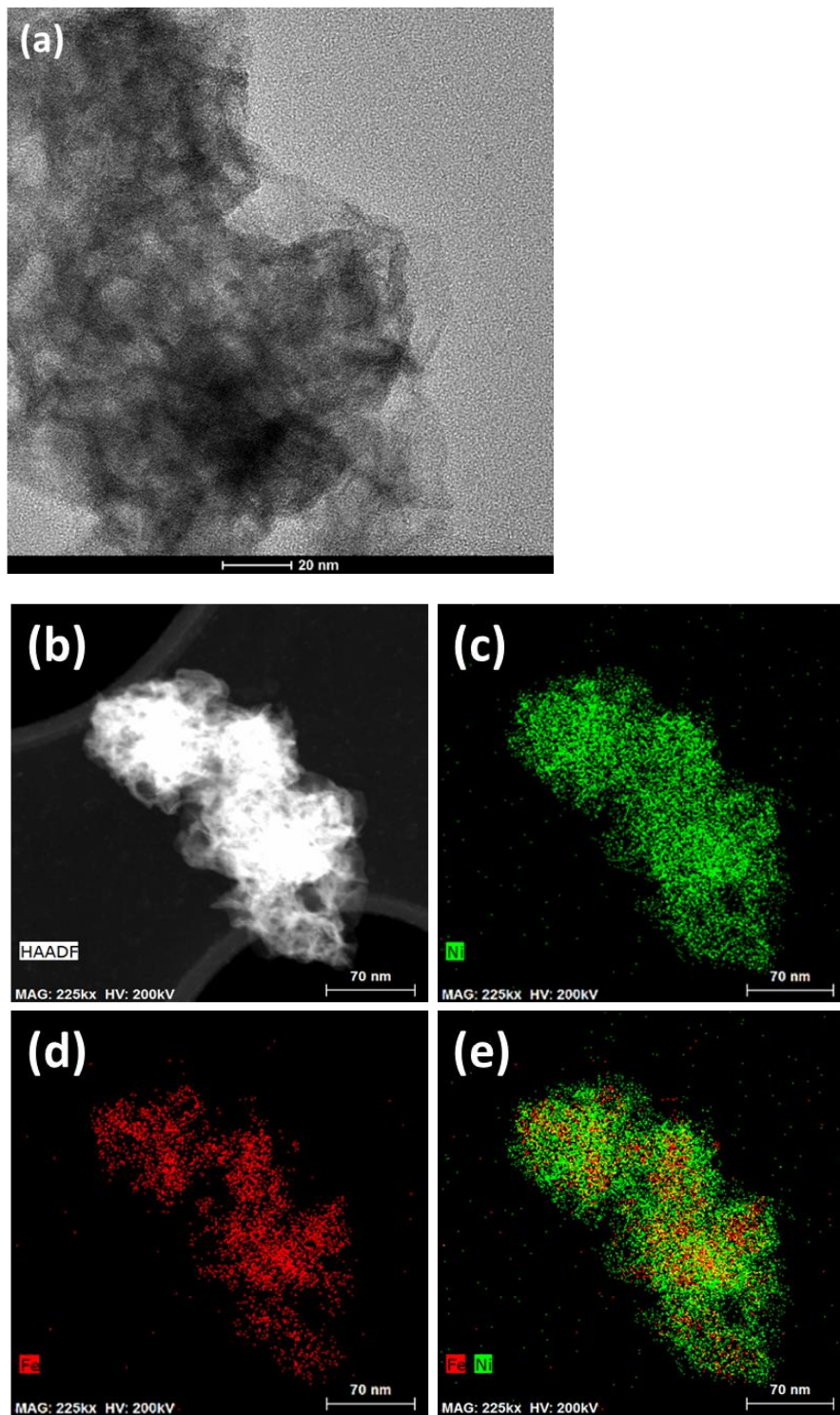


Figure S2 Microscopic characterization of FeOOH-NiOOH: (a) TEM, (b) HAADF-STEM, (c-e) corresponding EDX mapping images of Ni, Fe and overlay of Ni and Fe.

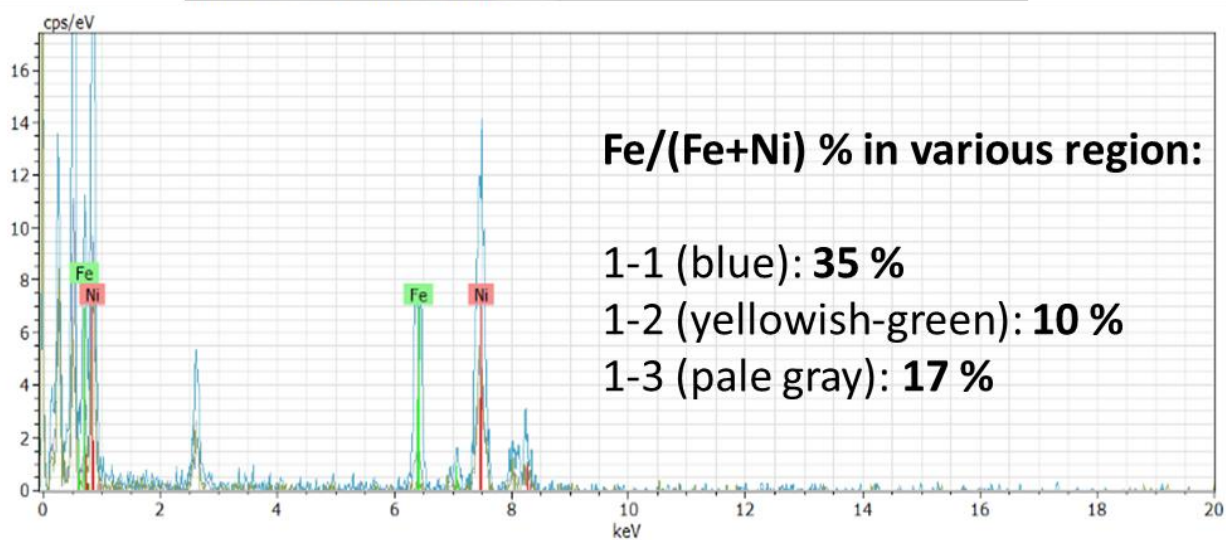
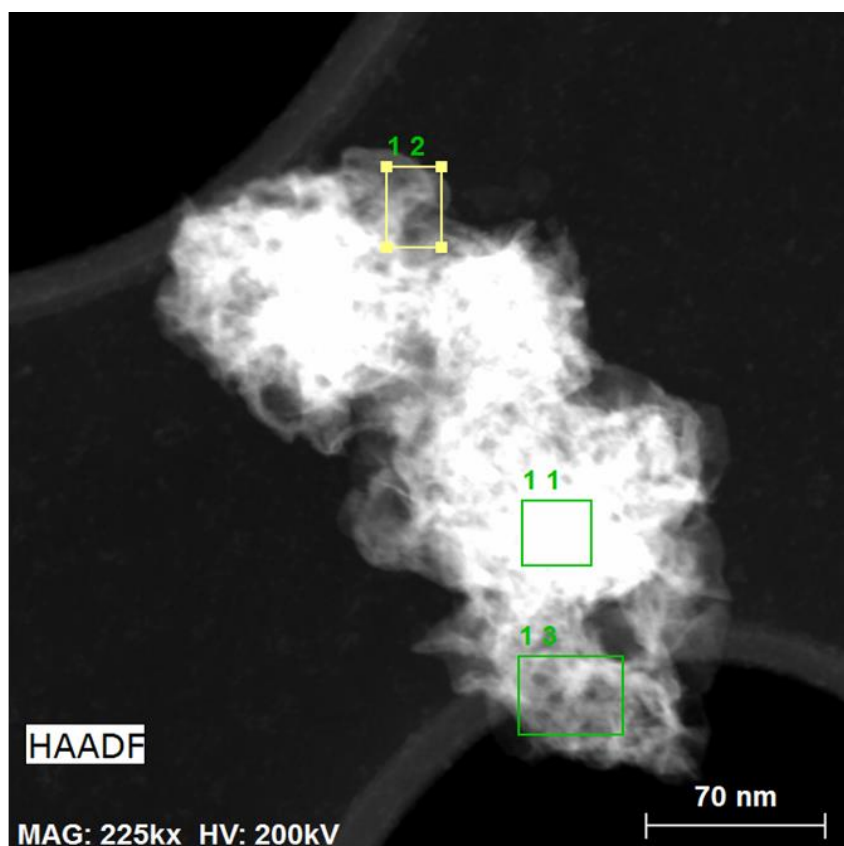


Figure S3 HAADF-STEM image of FeOOH-NiOOH (upper) and the corresponding EDX spectra of different regions (lower). The color of the curves: 1-1 blue; 1-2 yellowish-green; 1-3 pale gray. The Fe/(Fe+Ni)% ratio is indicated in the lower EDX spectra.

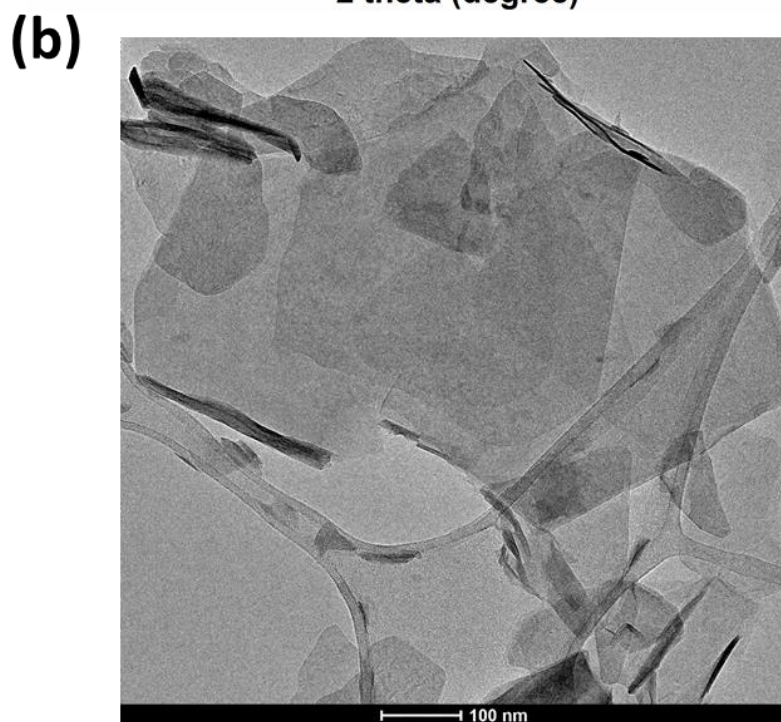
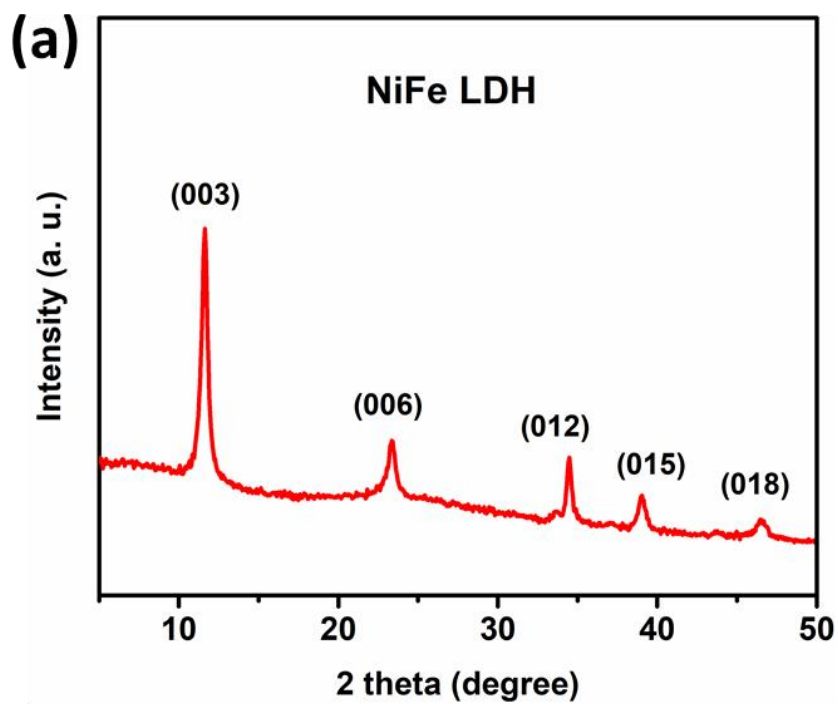


Figure S4 (a) PXRD and (b) TEM images of NiFe LDH (20% Fe, the following NiFe LDH samples are all based on this Fe content unless indicated otherwise).

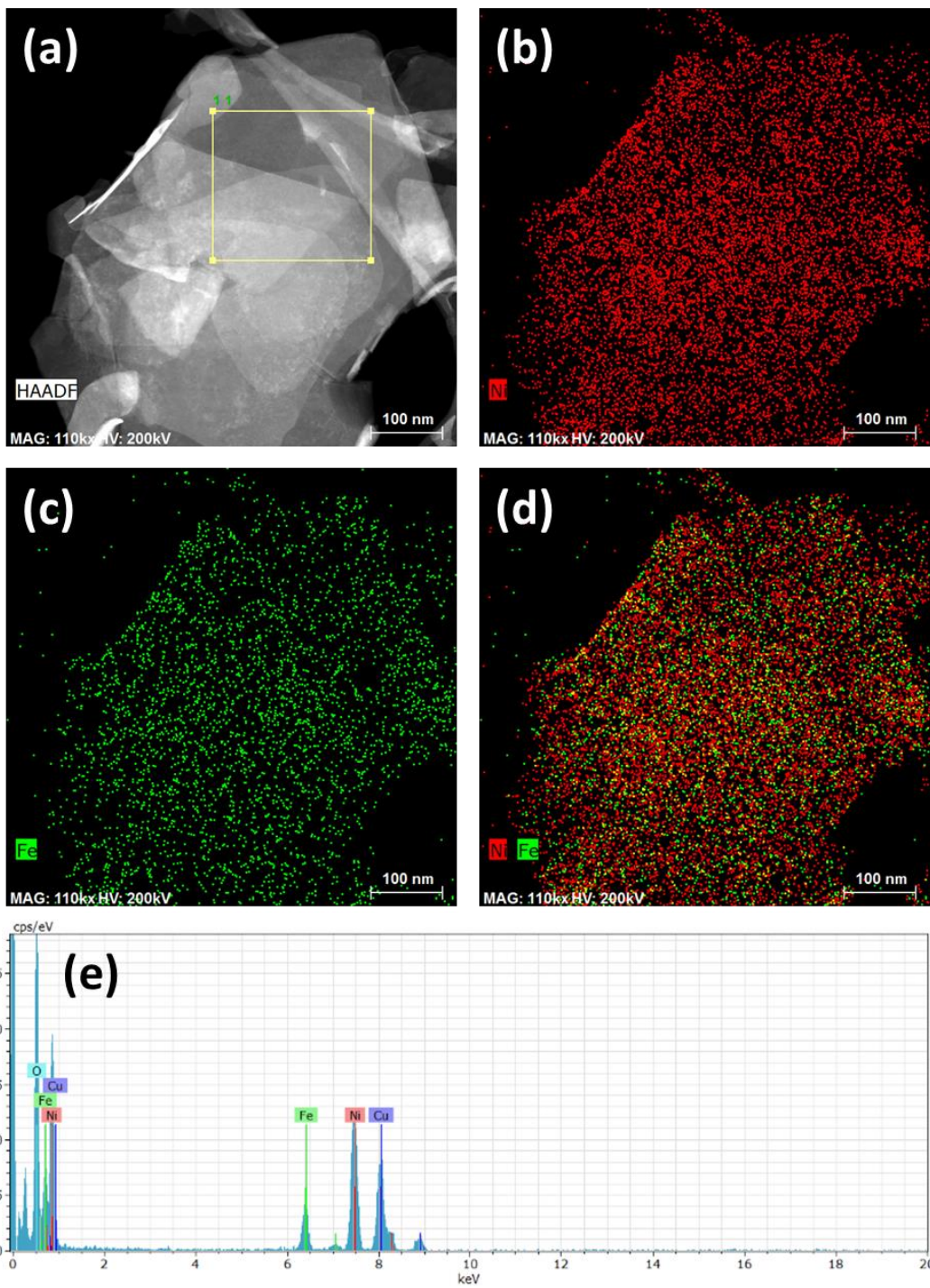


Figure S5 (a) HAADF-STEM image of NiFe LDH. (b-d) EDX mapping images of NiFe LDH: (b) Ni signals; (c) Fe signals; (d) overlay signals of Ni and Fe. (e) EDX mapping of the region in (a), suggesting Fe/(Fe+Ni)% ratio of 22 ± 2 %.

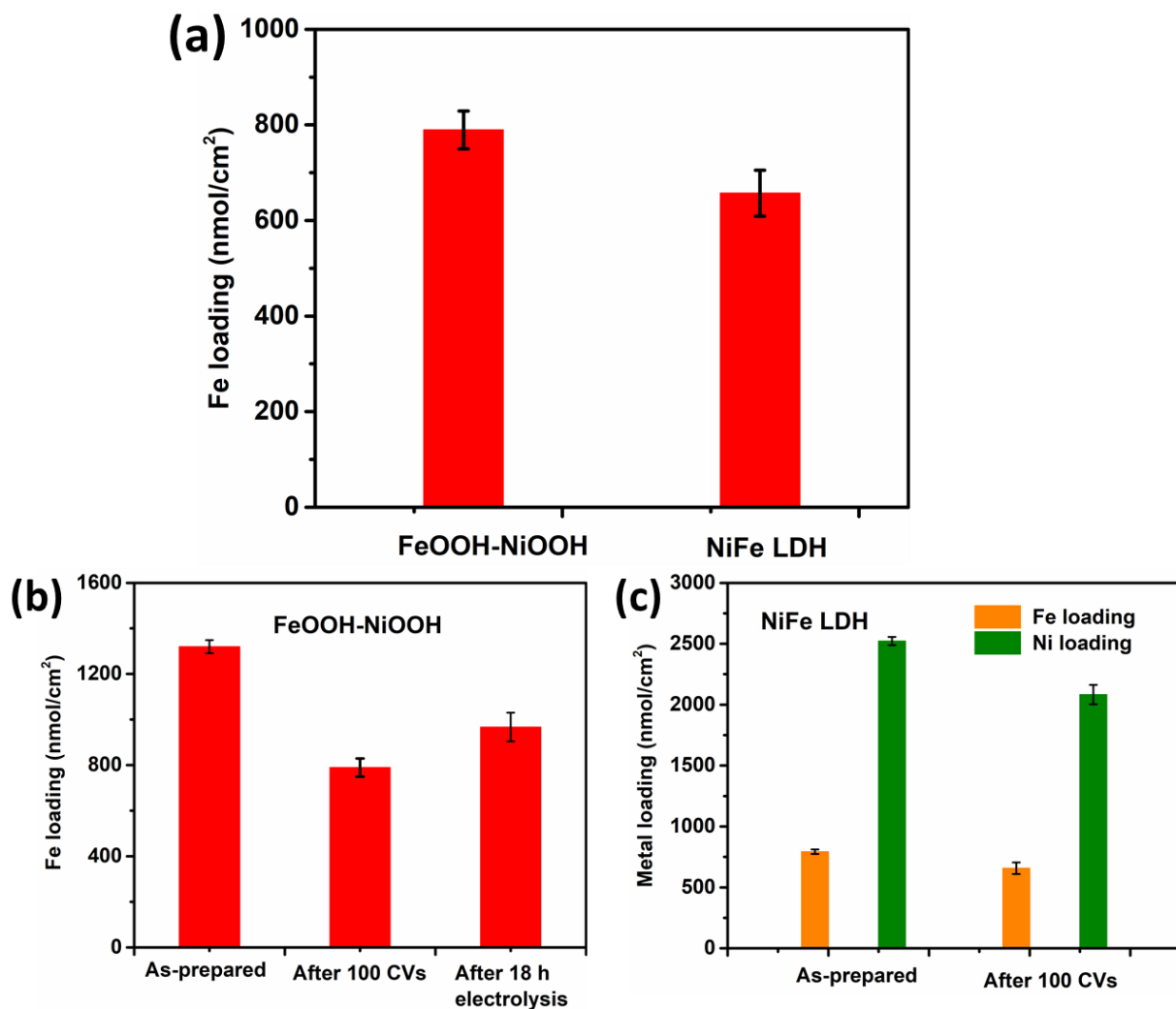


Figure S6 ICP-AES measurements. (a) Fe loadings of FeOOH-NiOOH and NiFe LDH after 100 CVs activation. (b) Variation of Fe loadings of FeOOH-NiOOH at different conditions. The slight increase of Fe loading after 18 h electrolysis is probably due to redeposition of Fe on nickel foam substrate. (c) Variation of Fe and Ni loadings of as prepared NiFe LDH and NiFe LDH after 100 CVs. The loading of both Ni and Fe slightly decreased due to the detachment of materials during reaction. The ratio of Fe/(Ni+Fe) is 23 ± 1 % for both as-prepared and activated samples, which is consistent with the results obtained from EDX spectra in Figure S5e and Figure S9e.

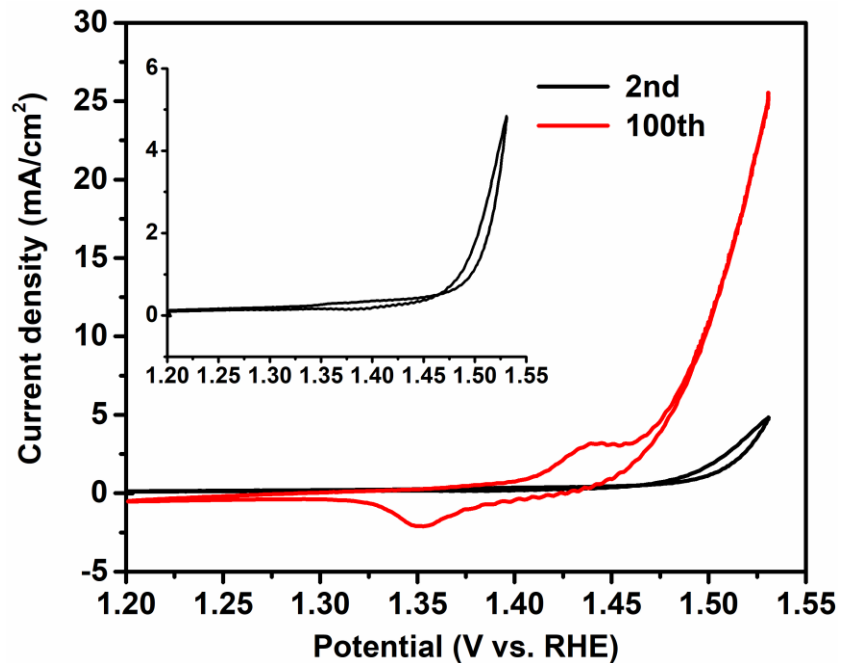


Figure S7 2nd and 100th CVs of NiFe LDH in 1 M KOH. Inset is the enlarged graph of the initial CV.

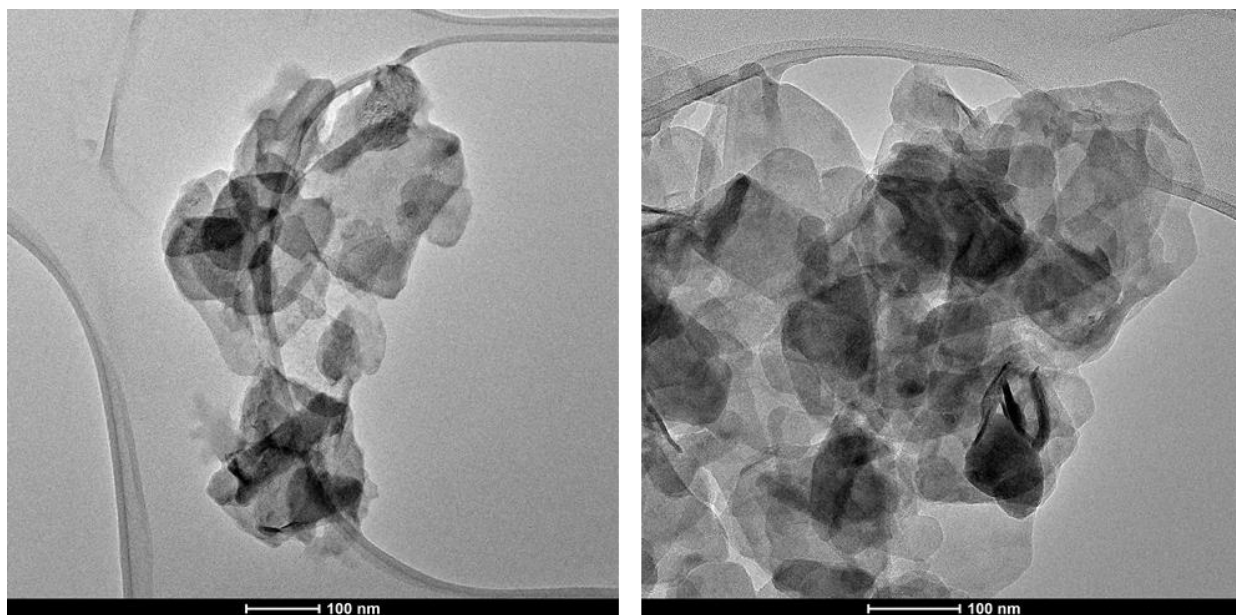


Figure S8 TEM images of NiFe LDH after activation by 100 CVs.

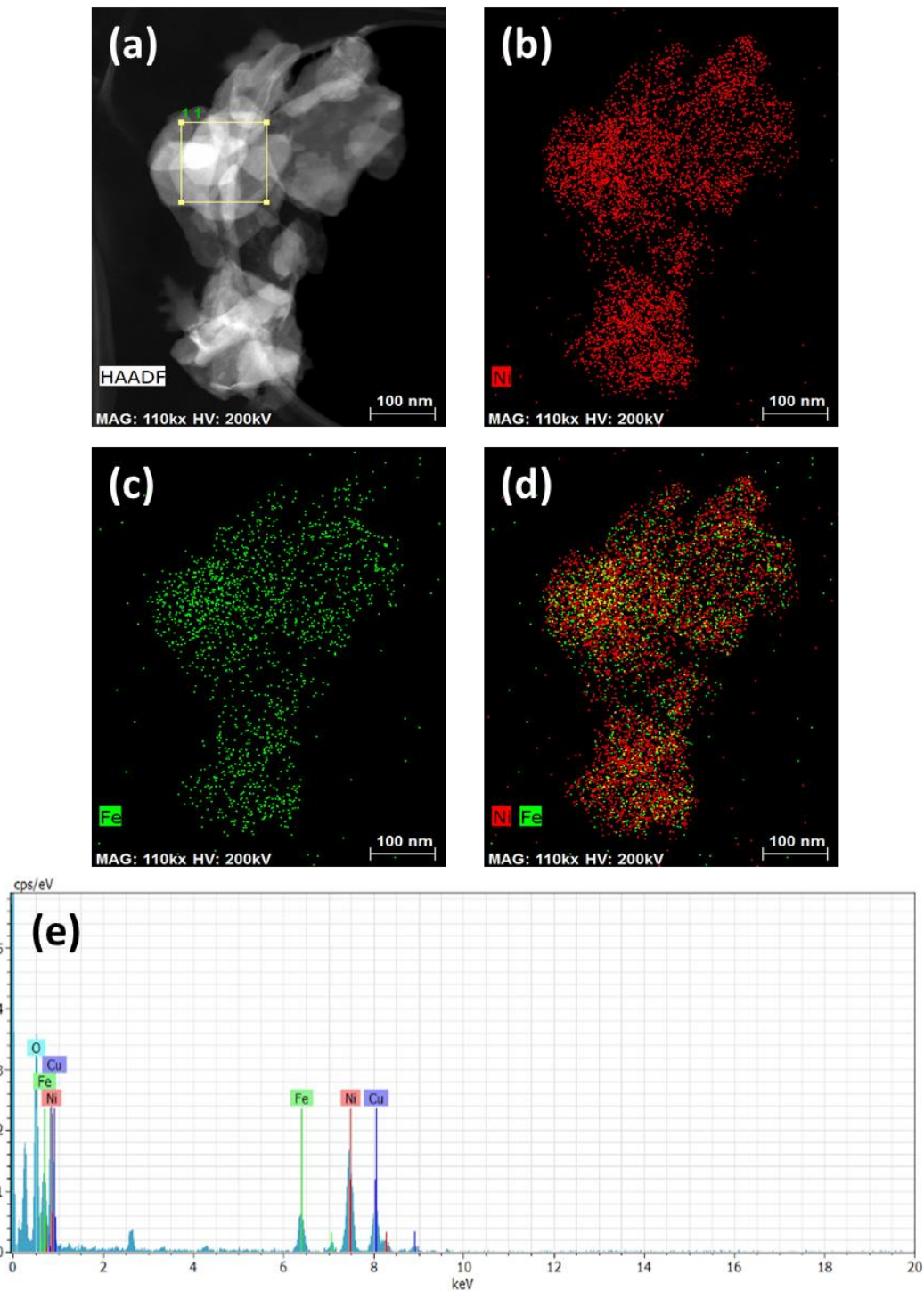


Figure S9 (a) HAADF-STEM image of NiFe LDH after activation. (b-d) EDX mapping images of NiFe LDH after activation: (b) Ni signals; (c) Fe signals; (d) overlay signals of Ni and Fe. (e) EDX mapping of the region in (a), suggesting Fe/(Fe+Ni)% ratio of 21 ± 2 %.

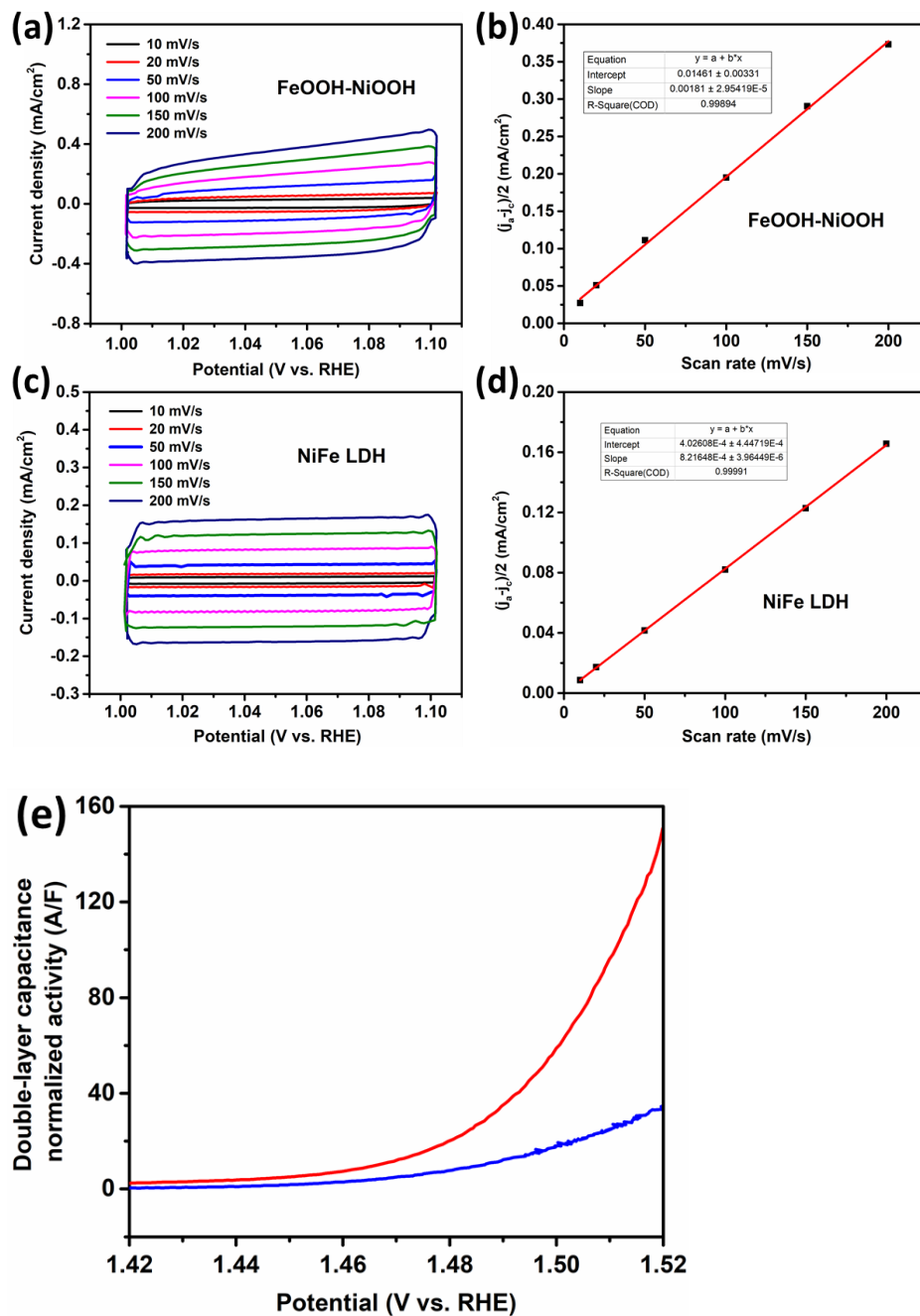


Figure S10 (a-d) Typical experiments for the determination of ECSA. CVs of (a) FeOOH-NiOOH and (c) NiFe LDH at different scan rates. The linear fit of half of the difference between anodic and cathodic current density versus scan rate for (b) FeOOH-NiOOH and (d) NiFe LDH. The slope is the double layer capacitance. Three independent experiments showed that the double layer capacitance of FeOOH-NiOOH is 1.97 ± 0.23 mF/cm², while that of NiFe LDH is 0.78 ± 0.11 mF/cm². (e) Double-layer capacitance normalized OER performance of FeOOH-NiOOH (red) and NiFe LDH (blue).

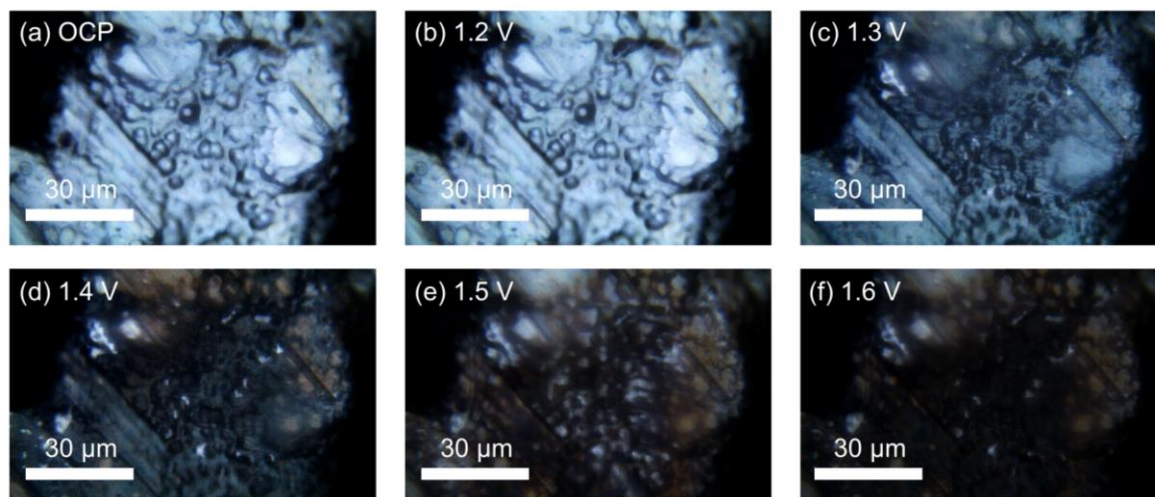


Figure S11 (a-f) Optical microscopy images of bare NF obtained from OCP to 1.6 V with an interval of 0.1 V.

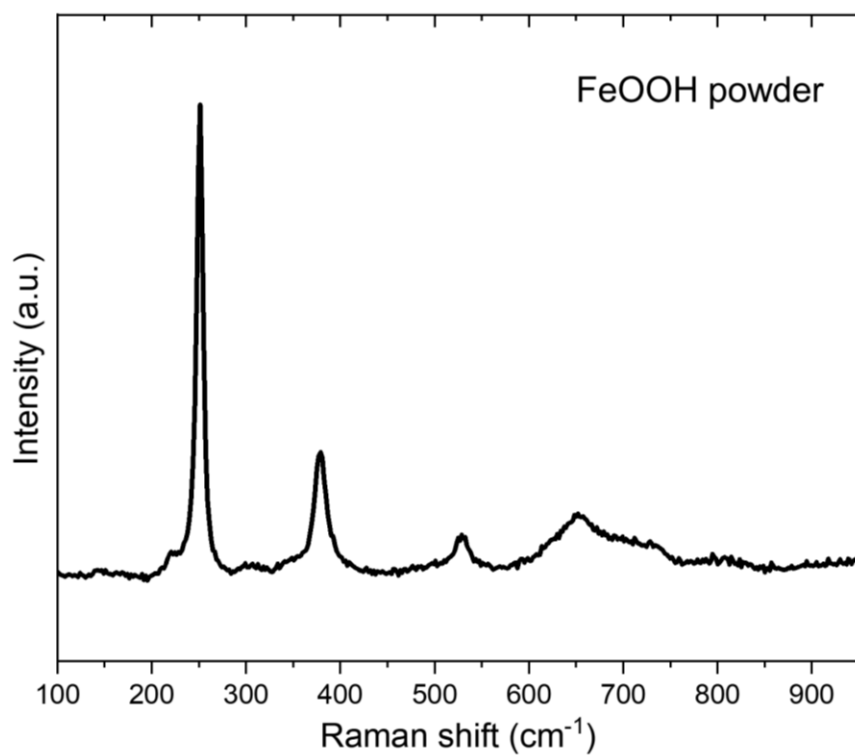


Figure S12 Ex-situ Raman spectrum of γ -FeOOH.

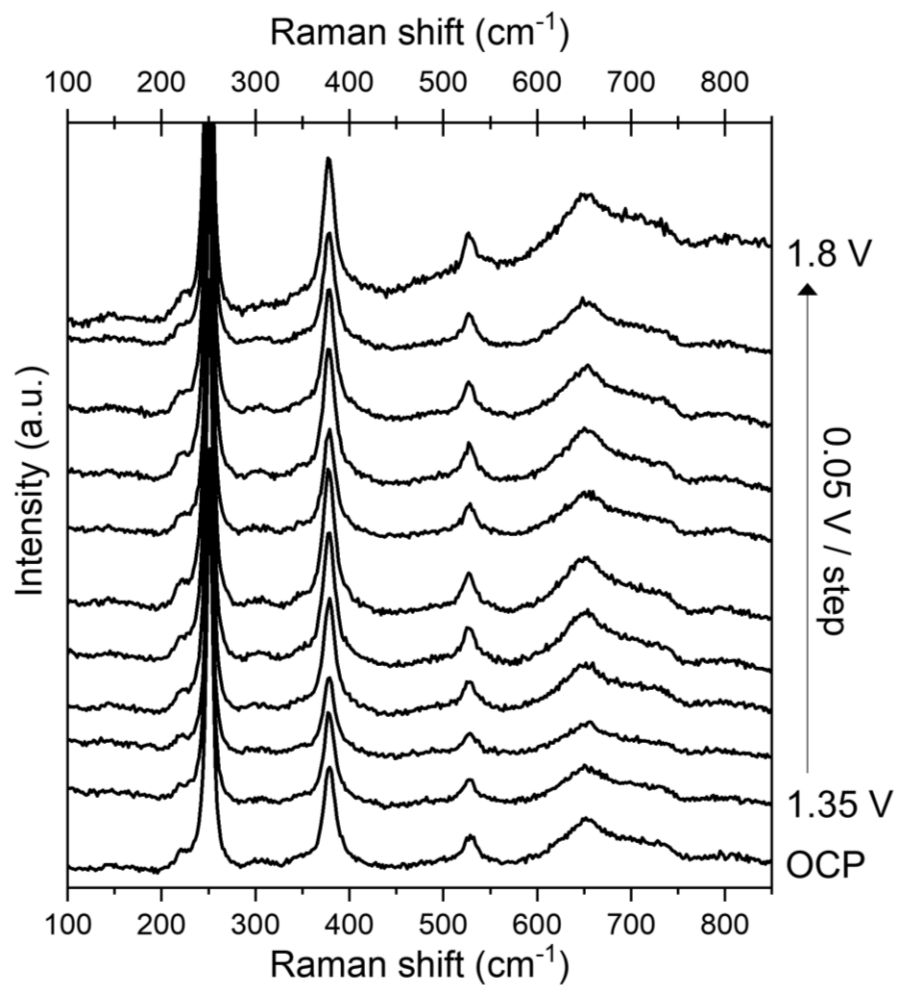


Figure S13. Operando Raman spectra of bare FeOOH obtained from OCP to 1.8 V in 1 M KOH.

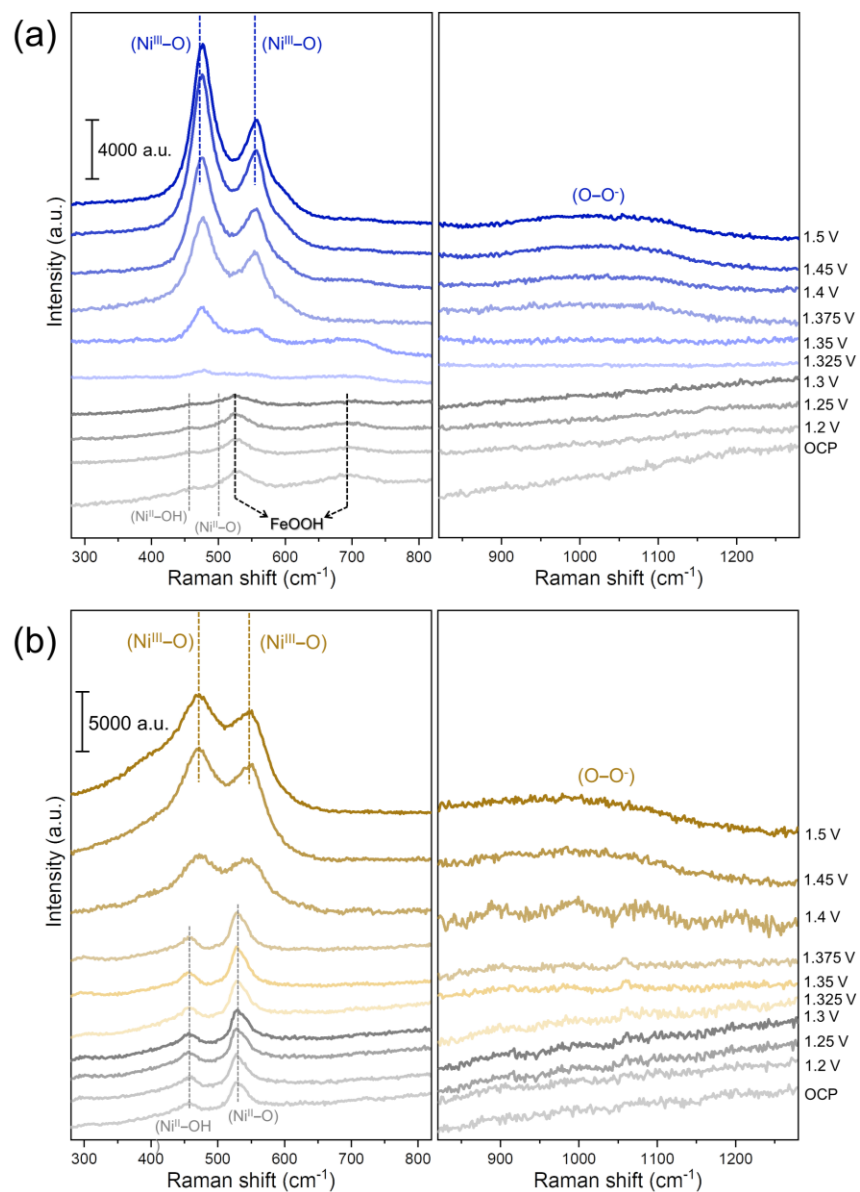


Figure S14 Operando Raman spectra of (a) FeOOH-NiOOH and (b) NiFe LDH recorded at given potentials.

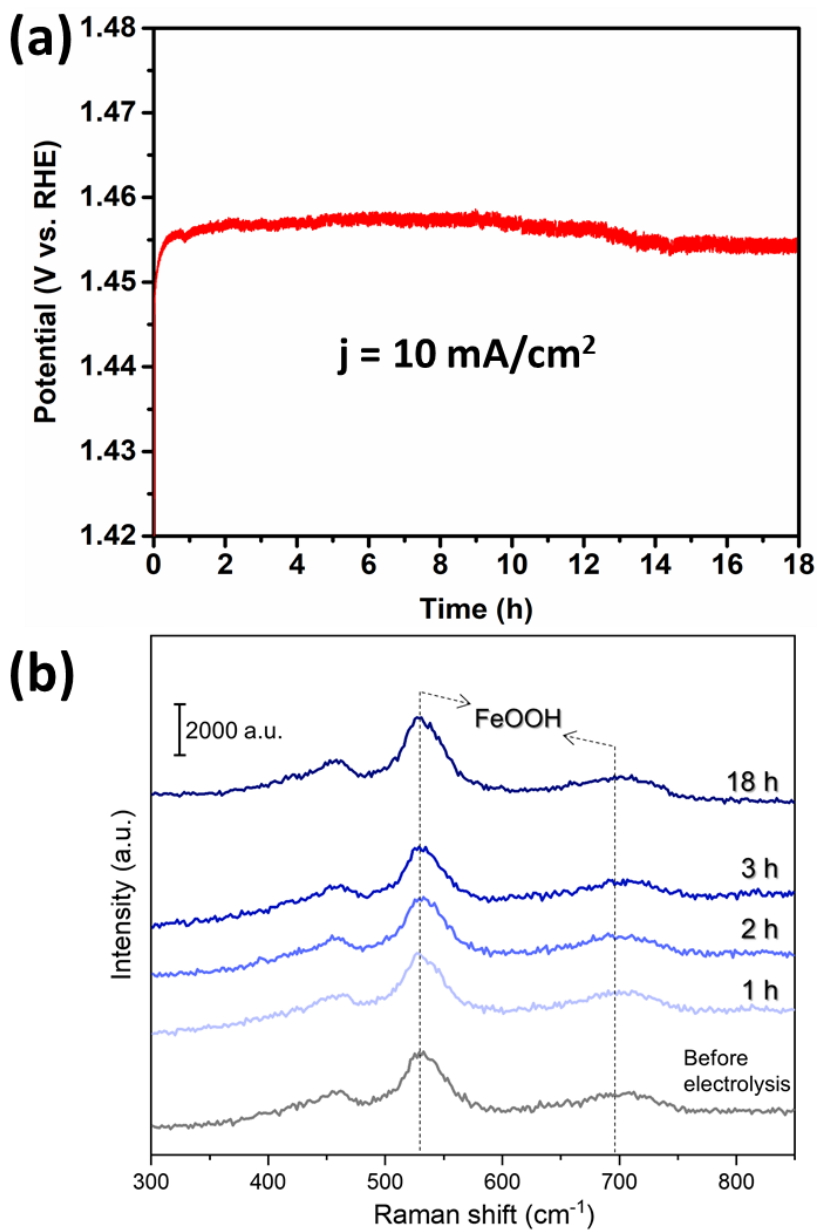


Figure S15. (a) Chronopotential electrolysis of FeOOH-NiOOH at 10 mA/cm^2 . The potential is corrected by ohmic loss. (b) Raman spectra of FeOOH-NiOOH recorded before and after 1h, 2h, 3h and 18h of electrolysis at a constant current of 10 mA cm^{-2} in 1 M KOH.

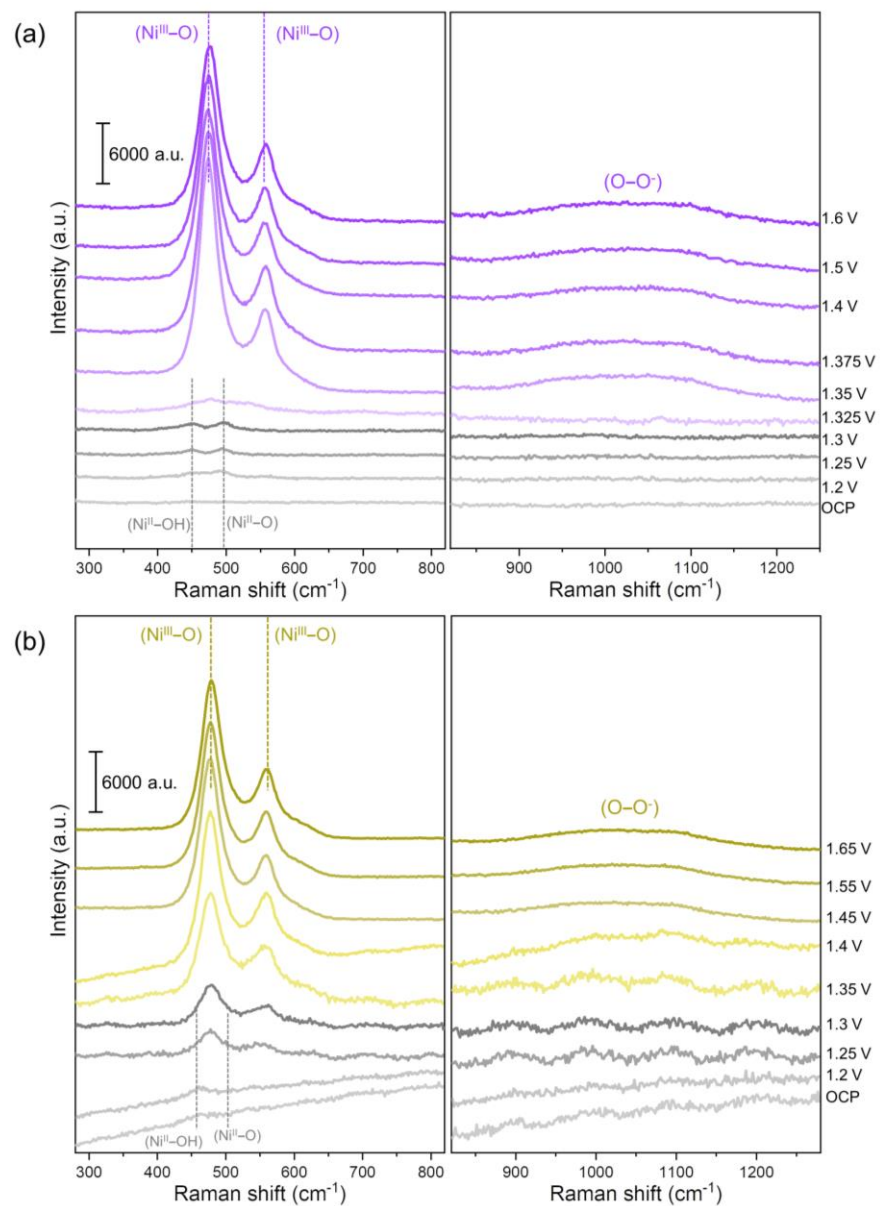


Figure S16 Operando Raman spectra of (a) bare NF and (b) Ni hydroxide recorded in the potential range of 1.2 V to 1.6 V and 1.65 V respectively.

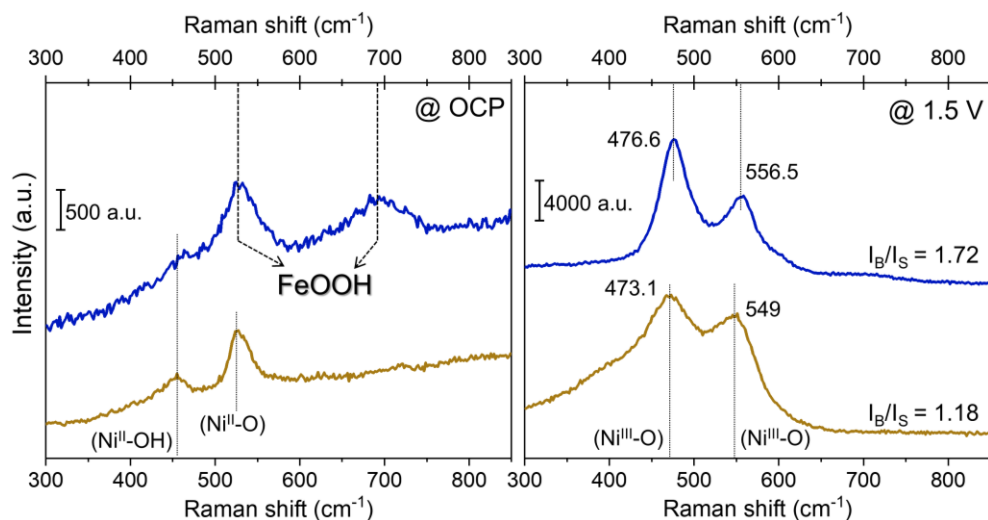


Figure S17. Operando Raman spectra of FeOOH-NiOOH (blue) and NiFe LDH (brown) recorded at OCP (left) and 1.5 V (right).

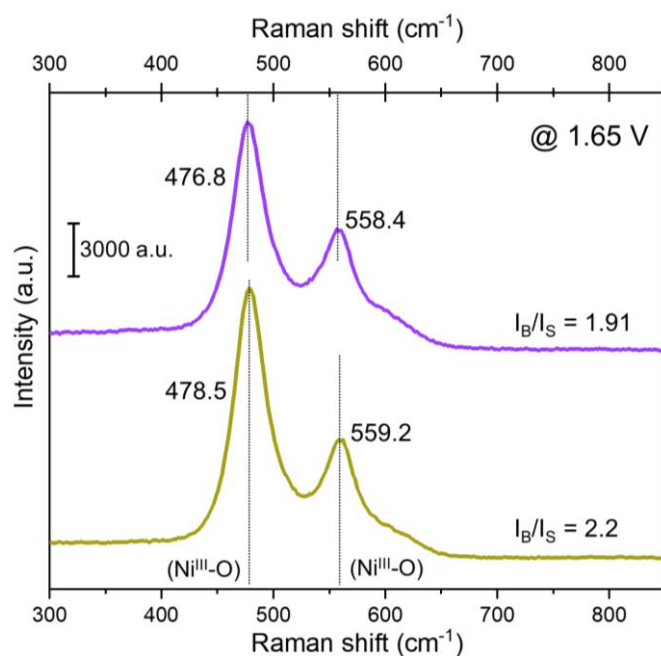


Figure S18 Operando Raman spectra of bare NF (purple) and Ni hydroxide (yellow green) measured at 1.65 V. The ratio of two main bands at 480 and 560 cm⁻¹ of each spectrum are indicated as I_B/I_S .

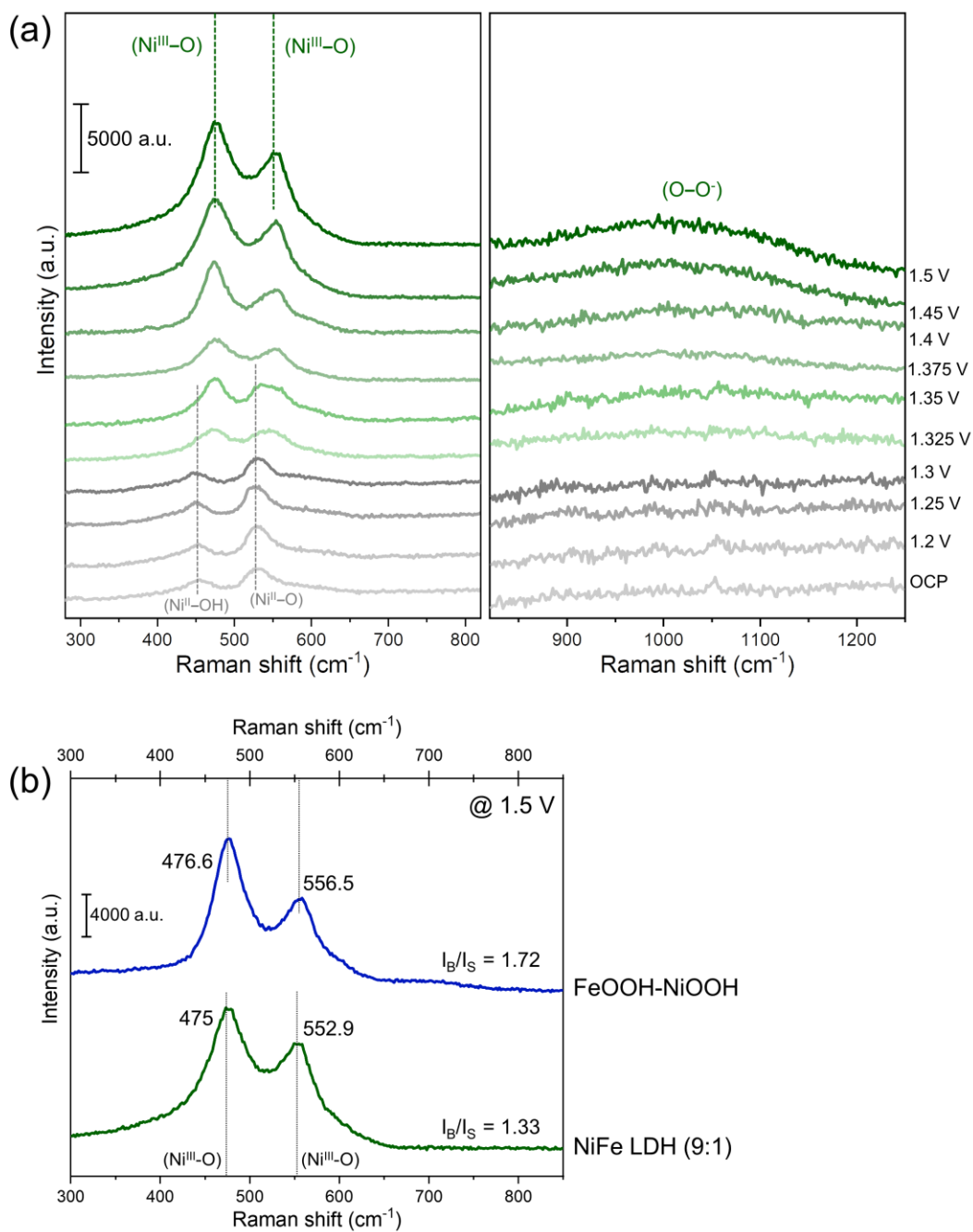


Figure S19 Operando Raman spectra of (a) NiFe LDH containing 10% of Fe at given potentials. (b) Operando Raman spectra of FeOOH-NiOOH (blue) and NiFe LDH (Fe 10%) (green) measured at 1.5 V. The ratio of two main bands of each spectrum are indicated as I_B/I_S .

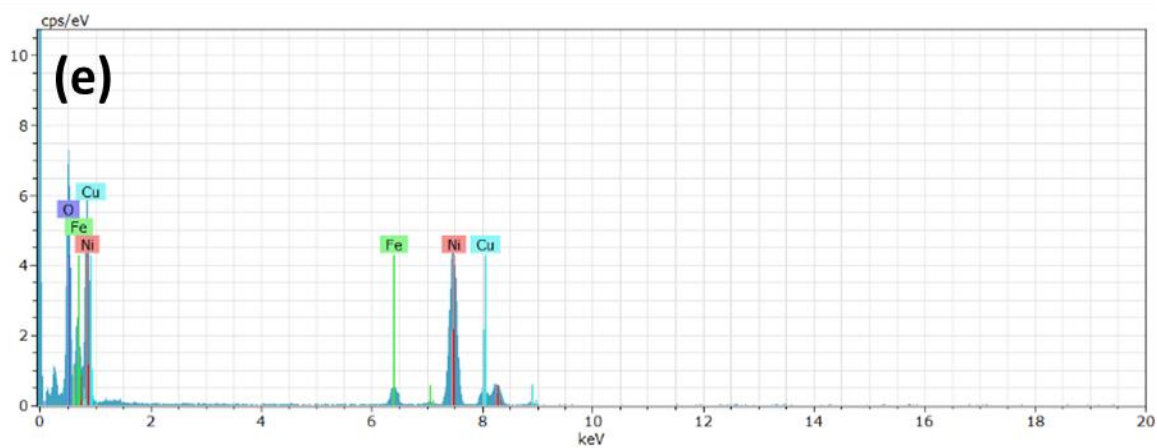
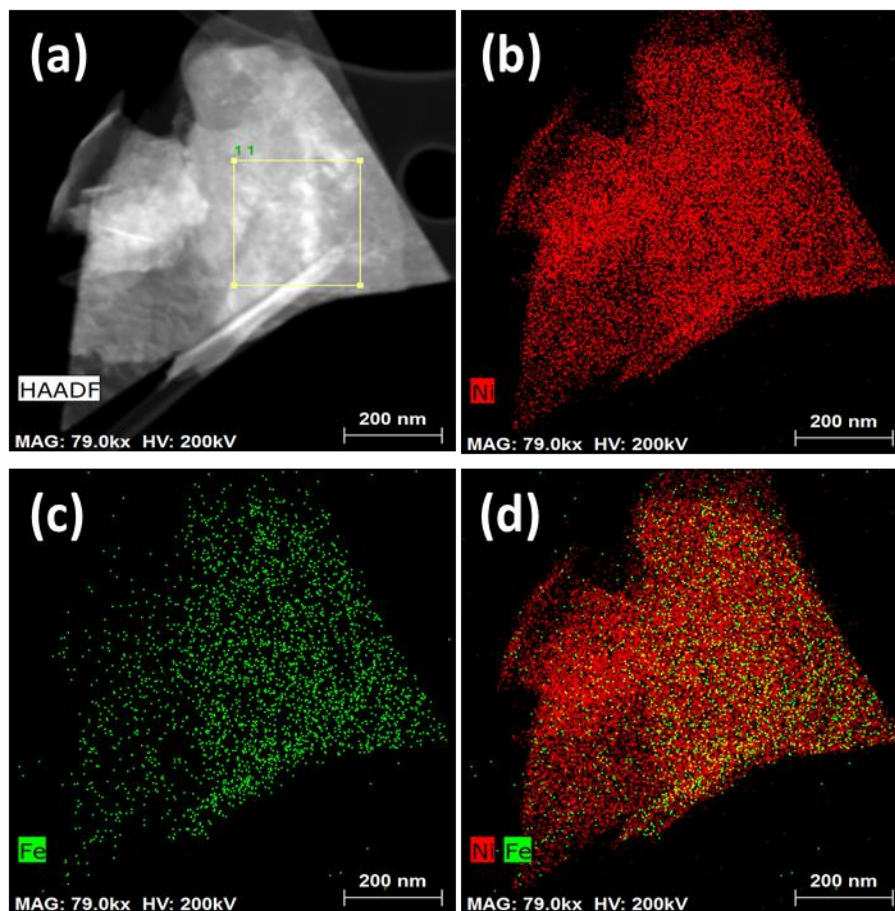


Figure S20 (a) HAADF-STEM image of NiFe LDH (10% Fe). (b-d) EDX mapping images of NiFe LDH (10% Fe): (b) Ni signals; (c) Fe signals; (d) overlay signals of Ni and Fe. (e) EDX mapping of the region in (a), suggesting Fe/(Fe+Ni)% ratio of 9 ± 2 %.

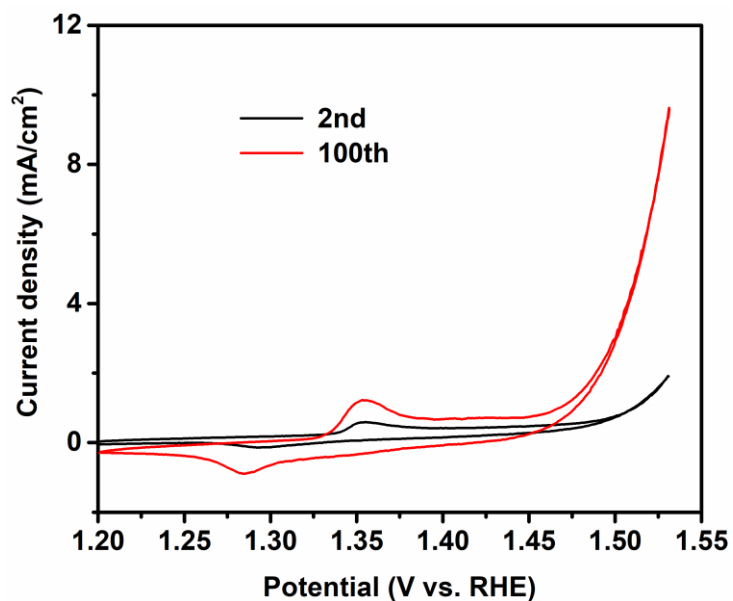


Figure S21 2nd and 100th CVs of NiFe LDH (10% Fe) in 1 M KOH.

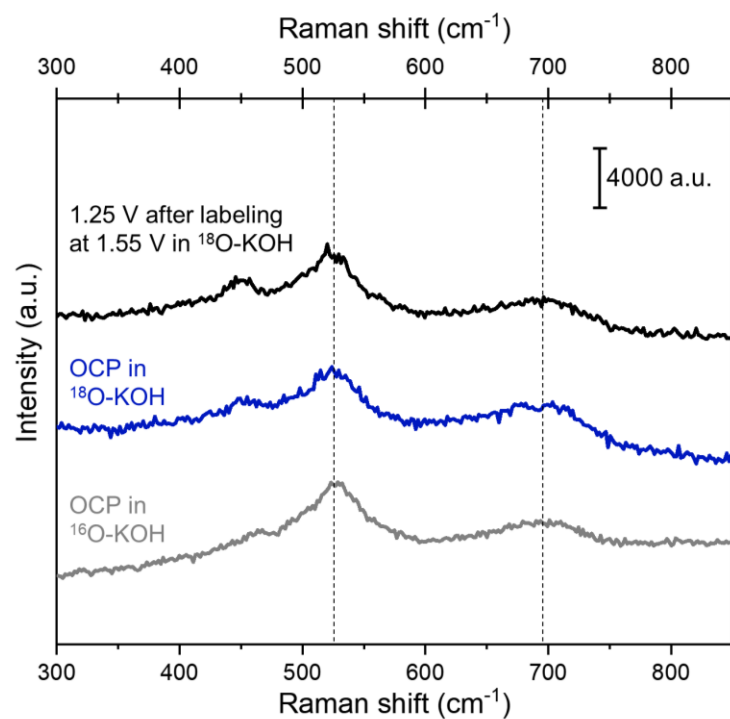


Figure S22. Operando Raman spectra of FeOOH-NiOOH (blue) obtained at OCP in ^{18}O -KOH before the labeling process and at 1.25 V after the activation for labeling by $^{18}\text{OH}^-$ at 1.55 V. The ^{16}O -labeled peaks of FeOOH at OCP in ^{16}O -KOH are indicated in grey at the bottom.

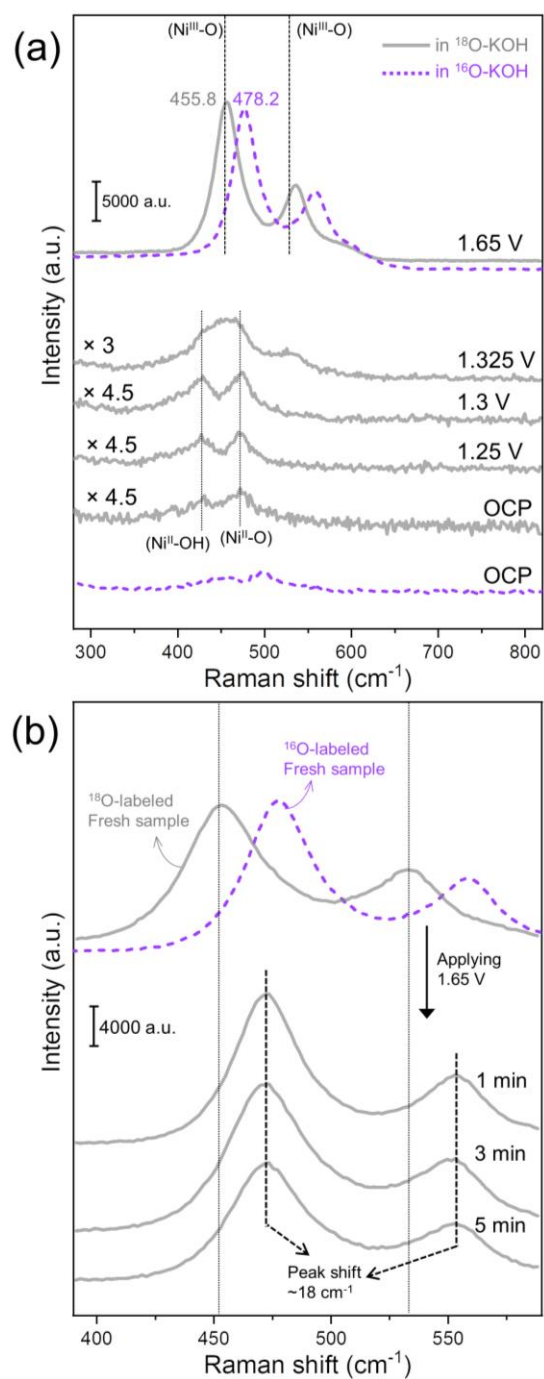


Figure S23 Operando Raman spectra of bare NF obtained at given potentials for oxygen isotope labeling (a) in 1 M KOH- H_2^{18}O solution and (b) subsequent isotope exchange experiment. The ^{18}O -labeled fresh sample was monitored at 1.65 V in 1 M KOH- H_2^{16}O solution. For ease of comparison of peak shift in between the two solutions, ^{16}O -labeled peaks are indicated in purple respectively.

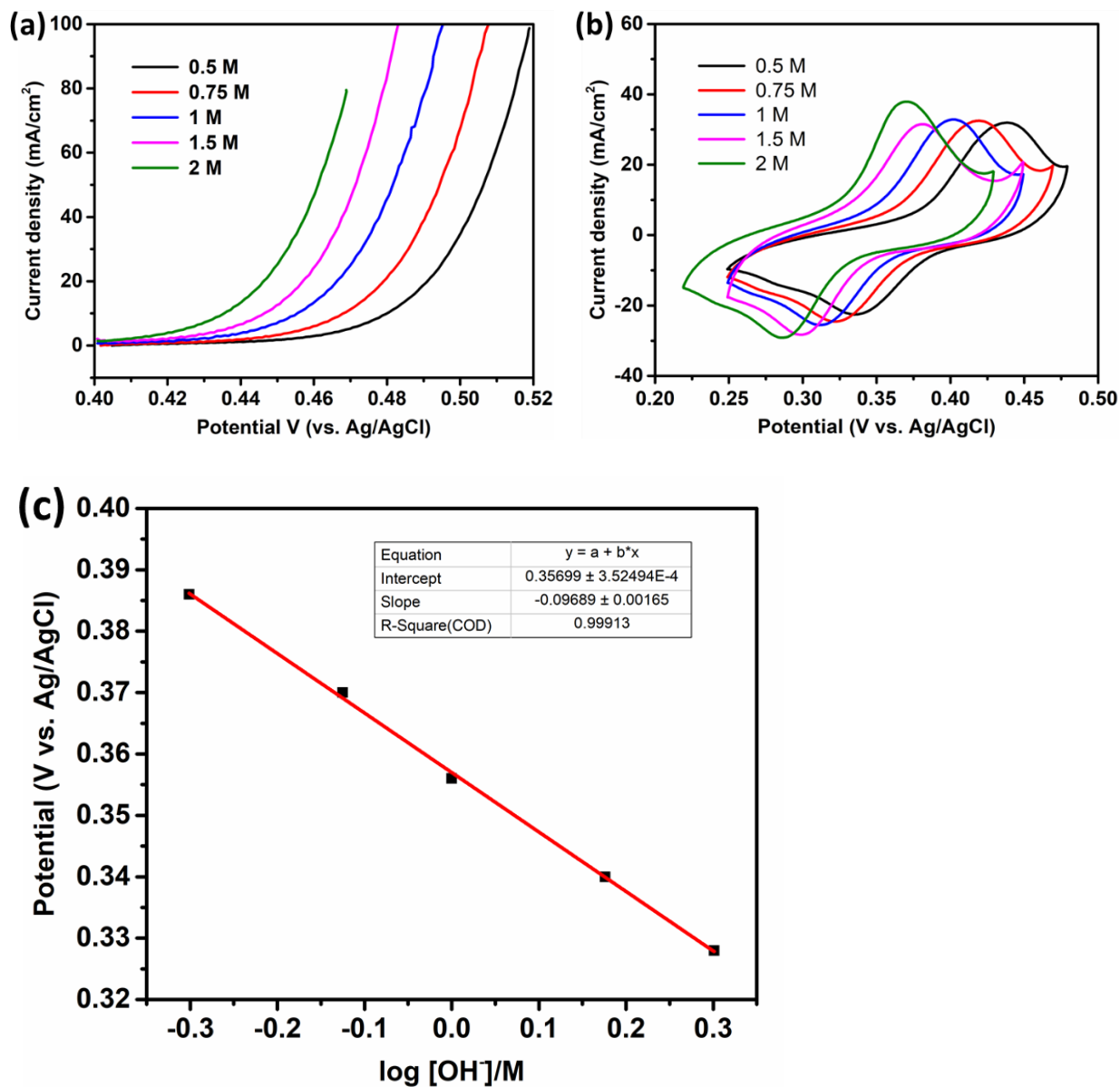


Figure S24 Electrokinetic study for FeOOH-NiOOH. (a) LSVs at various concentrations of KOH. (b) CVs at various concentrations of KOH. (c) The relationship of Ni(II)/Ni(III) redox potential based on the logarithm of the concentration of hydroxyl ions. Ni(II)/Ni(III) redox potential is derived from (b) by averaging the potential of oxidative and reductive peaks.

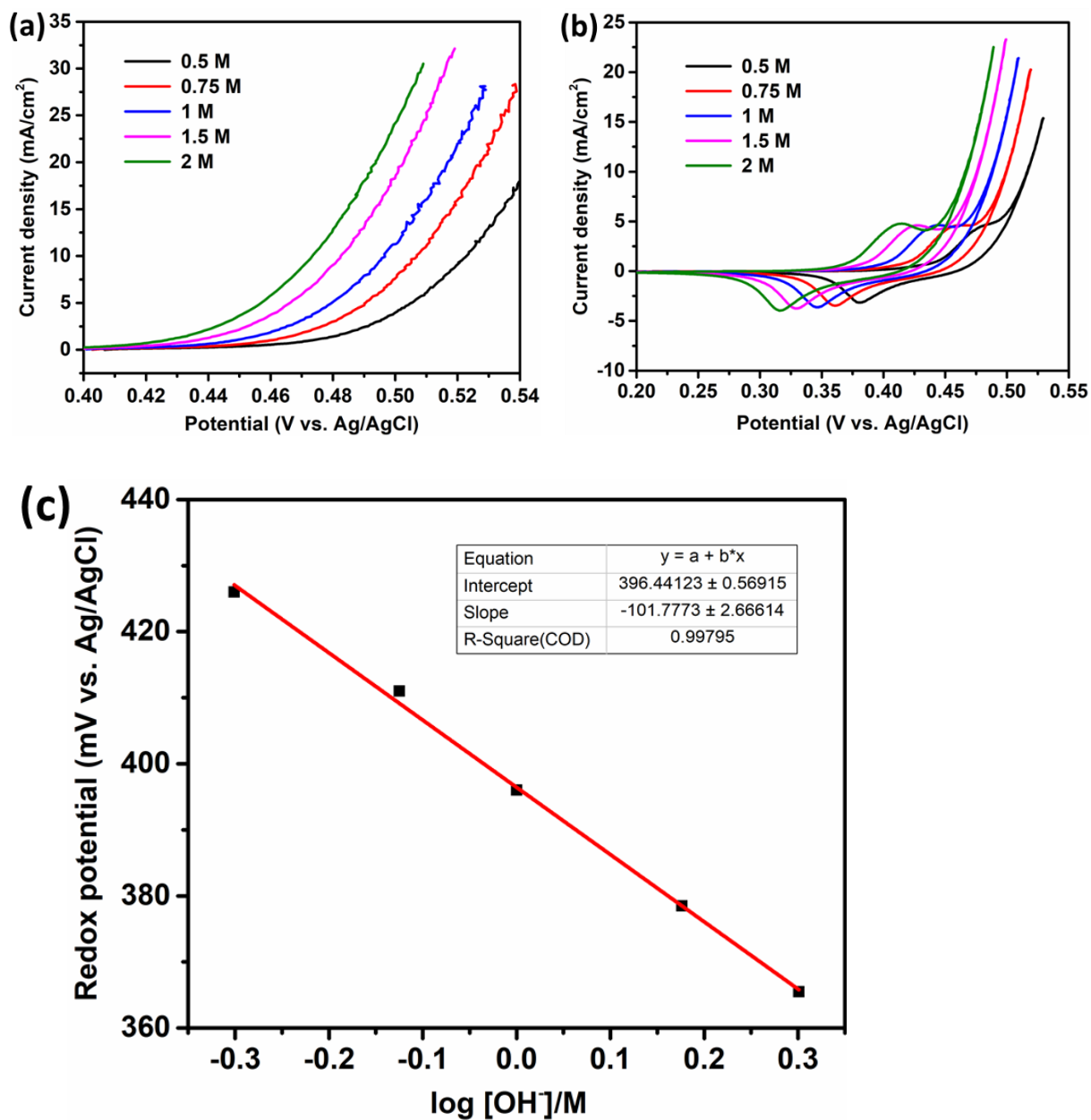


Figure S25 Electrokinetics study for NiFe LDH. (a) LSVs at various concentrations of KOH. (b) CVs at various concentrations of KOH. (c) The relationship of Ni(II)/Ni(III) redox potential based on the logarithm of the concentration of hydroxyl ions. Ni(II)/Ni(III) redox potential is derived from (b) by averaging the potential of oxidative and reductive peaks. For the catalyst in 0.5 M KOH, the oxidative peaks position is determined by looking for the point corresponding to lowest value of the first derivative of the forward CV scan (potential region: 0.45-0.52 V vs. Ag/AgCl).

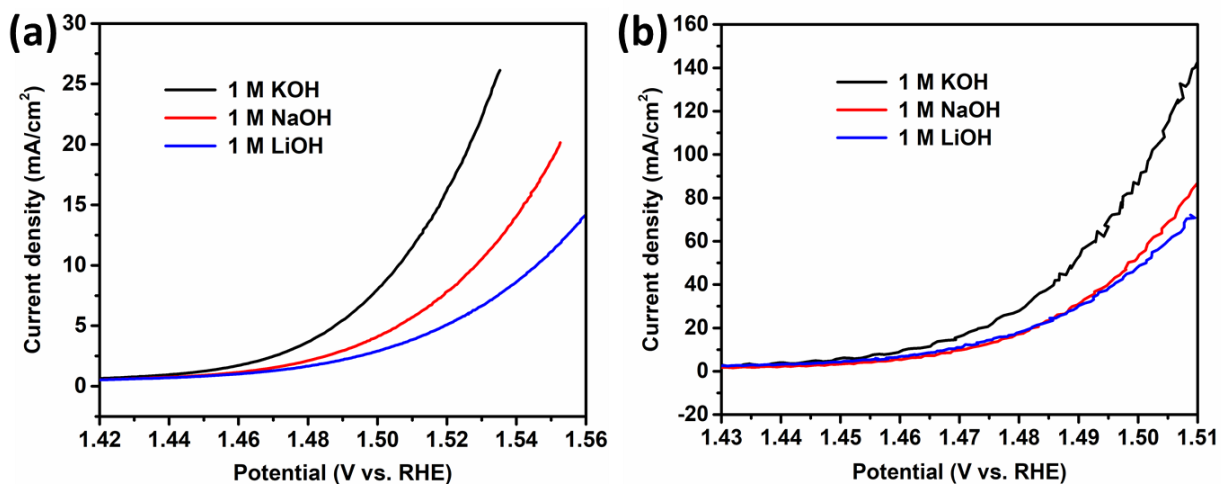


Figure S26 (a) Comparison of LSVs of NiFe LDH in 1 M KOH (black), 1 M NaOH (red) and 1 M LiOH (blue). (b) Comparison of LSVs of FeOOH-NiOOH in 1 M KOH (black), 1 M NaOH (red) and 1 M LiOH (blue).

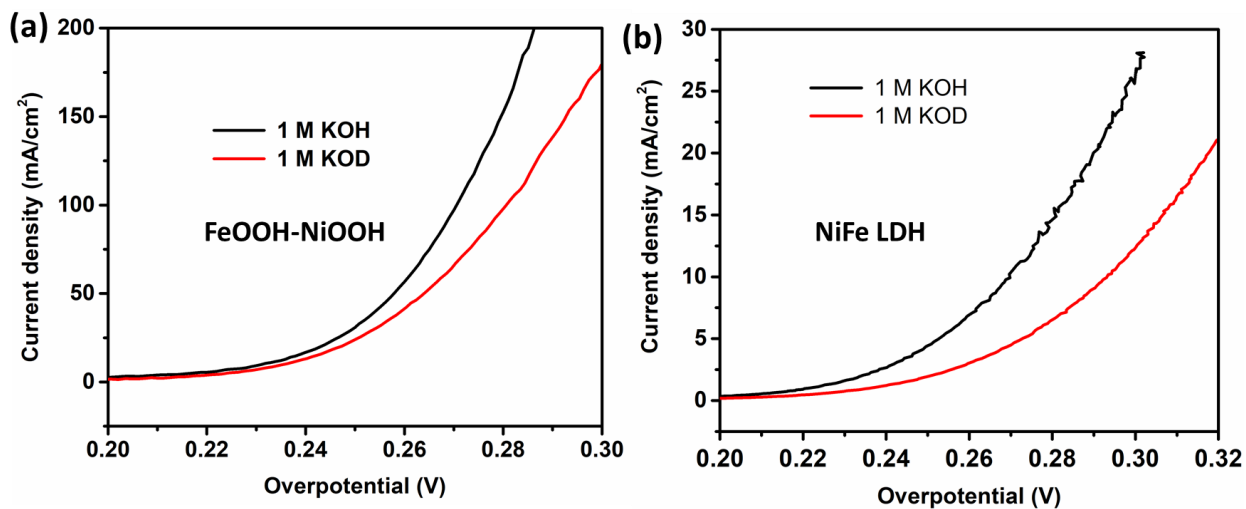


Figure S27 (a) A typical comparison of LSVs of FeOOH-NiOOH in 1 M KOH (black), 1 M KOD (red). (b) A typical comparison of LSVs of NiFe LDH in 1 M KOH (black), 1 M KOD (red).

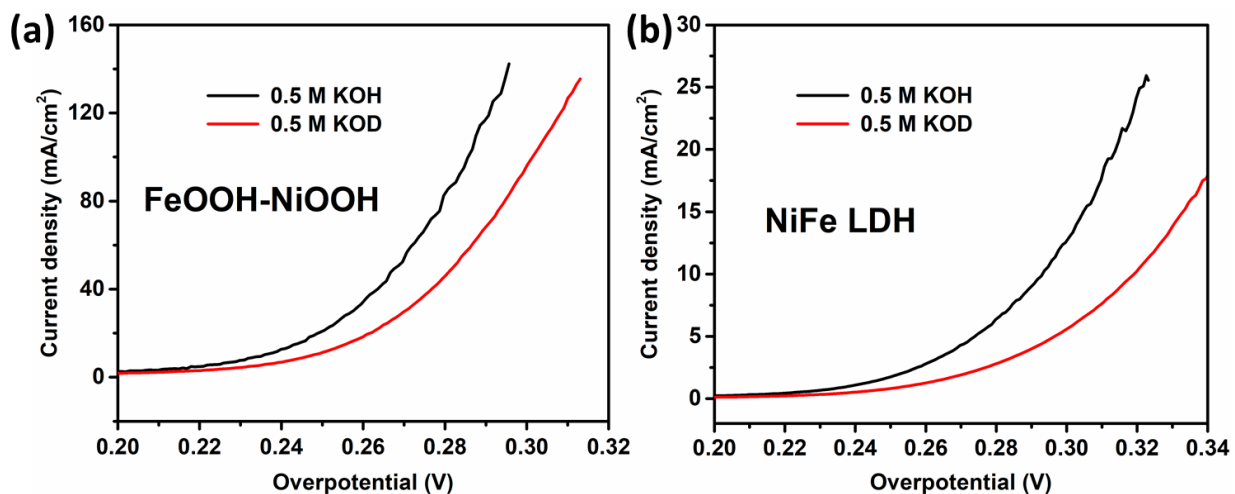


Figure S28 (a) A typical comparison of LSVs of FeOOH-NiOOH in 0.5 M KOH (black), 0.5 M KOD (red). (b) A typical comparison of LSVs of NiFe LDH in 0.5 M KOH (black), 0.5 M KOD (red).

Table S1 Tafel slope (mV/dec) of FeOOH-NiOOH and NiFe LDH in KOH with different concentrations.

[OH ⁻]	0.5M	0.75M	1M	1.5M	2M
FeOOH-NiOOH	39±1	38±1	38±2	37±1	37±1
NiFe LDH	47±2	46±3	43±2	43±2	42±2

Appendix 1 The quasi-equilibrium model for electrokinetic study

1.1 Bultler-Volmer equation

For any elemental electrochemical reaction ($xR \rightarrow yO + ne^-$), the catalytic current density can be described by Butler-Volmer equation:

$$j = nF(C_R^x k_a^0 \exp\left(\frac{n\alpha FE}{RT}\right) - C_O^y k_c^0 \exp\left(-\frac{n(1-\alpha)FE}{RT}\right)) \quad (S8)$$

In this equation, α is the transfer coefficient of the reaction, E is the applied potential, F is the Faraday constant, R is the universal gas constant, T is the thermodynamic temperature. Noted that E value is relative to Standard Hydrogen Electrode (SHE), which is zero point. C_R and C_O are concentration of reactant and product, respectively. k_a^0 and k_c^0 are rate constant of forward and reverse reaction, respectively. The subscript a and c are related to anodic and cathodic reactions. The expression of k_a^0 and k_c^0 are depicted as below:

$$k_a^0 = P_a \exp\left(\frac{-\Delta\widetilde{G}_a^0(E=0)}{RT}\right) \quad (S9)$$

$$k_c^0 = P_c \exp\left(\frac{-\Delta\widetilde{G}_c^0(E=0)}{RT}\right) \quad (S10)$$

The $\Delta\widetilde{G}_a^0(E=0)$ and $\Delta\widetilde{G}_c^0(E=0)$ denote as standard Gibbs free energy of activation, which are related to the activation energies (energy barriers) to be overcome by the reduced (a) and oxidized (c) species in standard conditions. P_a and P_c are corresponding pre-exponential factors. Noted that both k_a^0 and k_c^0 are related to standard condition, which is independent of the concentration of reduced and oxidized species.

At the equilibrium potential (E_{eq}), the forward and reverse reaction rate is equal ($j_a = j_c$). Then,

$$C_{Req}^x k_a^0 \exp\left(\frac{n\alpha FE_{eq}}{RT}\right) = C_{Oeq}^y k_c^0 \exp\left(-\frac{n(1-\alpha)FE_{eq}}{RT}\right) \quad (S11)$$

In this case the Butler-Volmer Equation is reformatted as:

$$j = j_0 \left(\frac{C_R^x}{C_{Req}^x} \exp\left(\frac{n\alpha F\eta}{RT}\right) - \frac{C_O^y}{C_{Oeq}^y} \exp\left(-\frac{n(1-\alpha)F\eta}{RT}\right) \right) \quad (S12)$$

$$j_0' = nFC_{Req}^x k_a^0 \exp\left(\frac{n\alpha FE_{eq}}{RT}\right) = nFC_{Oeq}^y k_c^0 \exp\left(-\frac{n(1-\alpha)FE_{eq}}{RT}\right) \quad (S13)$$

$$\eta = E - E_{eq} \quad (S14)$$

η is the applied overpotential. When the reaction is highly irreversible, the Eq. S12 is reformatted as well-known Tafel equation, j_0 is the exchange current density:

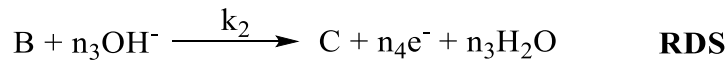
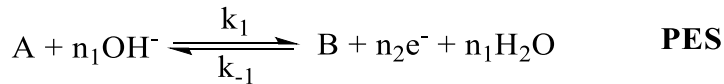
$$j = j_0 \exp\left(\frac{n\alpha F\eta}{RT}\right) \quad (S15)$$

$$j_0 = nFC_R^x k_a^0 \exp\left(\frac{n\alpha FE_{eq}}{RT}\right) = nFk_a C_R^x \quad (S16)$$

$$k_a = k_a^0 \exp\left(\frac{n\alpha FE_{eq}}{RT}\right) \quad (S17)$$

1.2 Quasi-Langmuir model

The mechanism of oxygen evolution reactions (OER) in the Tafel region can be described by a quasi-Langmuir model.^[8] In this model, the surface concentration of key intermediate (resting state) is less than 10%, which fits the general condition of Langmuir isotherm adsorption. This assumption is reasonable when the applied potential is moderate (e.g. in the Tafel region). Generally, the key process of OER involves a pre-equilibrium (quasi-equilibrium) step (PES) and a rate-determining step (RDS). In alkaline condition, the reactions were depicted as Scheme S1. The PES can either be a single electrochemical step (in most case $n_2 = 1$) or combined consecutive electrochemical steps ($n_2 \geq 1$). For the RDS, the transferred electrons n_4 can be either 1 or 0. The overall rate of the OER is related to these two steps, while the other steps such as the reversible redox processes (can be described by Nernst equation, see below) and the processes after RDS will not restrict the final reaction rate.^[9]



Scheme S1. General key process in alkaline OER.

k_1 and k_{-1} are the rate constants of the forward and reverse reaction of PES, respectively. k_2 is rate constants of RDS. The steady-state velocity of oxygen evolution can be expressed as follows by using Butler-Volmer equation:

$$v = k_2 \theta_B a_{OH^-}^{n_3} \exp\left(\frac{n_4 \alpha_2 \eta_2 F}{RT}\right) \quad (S18)$$

α_2 is the transfer coefficient of RDS, η_2 is the overpotential relative to equilibrium potential of RDS (it is not equal to apparent overpotential relative to OER equilibrium potential), F is the Faraday constant, R is the universal gas constant, T is the thermodynamic temperature. θ_B represents the partial surface coverage of intermediate B . θ_B can be defined in terms of the surface coverage of the resting state A (θ_A). The relationship between θ_B and θ_A can be deduced from the equilibrium equation:

$$v_a = k_1 \theta_A a_{OH^-}^{n_1} \exp\left(\frac{n_2 \alpha_1 \eta_1 F}{RT}\right) \quad (S19)$$

$$v_{-a} = k_{-1}\theta_B \exp\left(-\frac{n_2(1-\alpha_1)\eta_1 F}{RT}\right) \quad (\text{S20})$$

For the quasi-equilibrium condition:

$$v_a = v_{-a} \quad (\text{S21})$$

η_1 is the overpotential relative to equilibrium potential of PES. Since both η_1 and η_2 are hard to determine, we use applied potential E and standard rate constants (denoted with superscript 0, similar as Eq. S17) to rearrange the above equation. Then we have:

$$\theta_B = K_1^0 \theta_A a_{OH^-}^{n_1} \exp\left(\frac{n_2 EF}{RT}\right) \quad (\text{S22})$$

$$K_1^0 = \frac{k_1^0}{k_{-1}^0}. \quad (\text{S23})$$

$$v = k_2^0 \theta_B a_{OH^-}^{n_3} \exp\left(\frac{n_4 \alpha_2 EF}{RT}\right) \quad (\text{S18}')$$

Substituting the expression of θ_B (Eq. S22) for Eq. S18', the steady-state velocity of OER can be expressed as:

$$v = k_2^0 K_1^0 \theta_A a_{OH^-}^{n_1+n_3} \exp\left(\frac{(n_2+n_4\alpha_2)EF}{RT}\right) \quad (\text{S24})$$

If Langmuir conditions are assumed, the surface coverage of A (θ_A) would not be expected to change appreciably over the potential range, and may be considered a potential-independent constant. The catalytic current density of OER is:

$$j = 4Fv = k^0 a_{OH^-}^{n_1+n_3} \exp\left(\frac{(n_2+n_4\alpha_2)EF}{RT}\right) \quad (\text{S25})$$

$$k^0 = 4Fk_2^0 K_1^0 \theta_A \quad (\text{S26})$$

The Tafel slope, $\left(\frac{\partial E}{\partial \log j}\right)_{pH}$ or $\left(\frac{\partial \eta}{\partial \log j}\right)_{pH}$, of OER can be expressed as:

$$\left(\frac{\partial E}{\partial \log j}\right)_{pH} = \left(\frac{\partial \eta}{\partial \log j}\right)_{pH} = \frac{2.303RT}{(n_2+n_4\alpha_2)F} \quad (\text{S27})$$

To study the order of proton concentration ($[H^+]$) or hydroxyl ions concentration ($[OH^-]$) on the reaction rate, according to Eq. S24, in principle we can directly measure current density at a certain potential E (relative to Standard Hydrogen Electrode, SHE, the standard condition) with changing the $[OH^-]$. However, the current density may not locate in Tafel region, making the determination inaccurate. Typically, we first measure the variation of the potential with changing $[OH^-]$ in a constant current density (in Tafel region). Then the order of $[OH^-]$ can be determined by Eq. S4.

$$\left(\frac{\partial \log j}{\partial \log [OH^-]}\right)_E = -\frac{\left(\frac{\partial E}{\partial \log [OH^-]}\right)_j}{\left(\frac{\partial E}{\partial \log j}\right)_{pH}} \quad (\text{S4})$$

The relationship is also correct when the E is substituted by η (Eq. S28), the $\left(\frac{\partial \log j}{\partial \log [\text{OH}^-]}\right)_\eta$ is pH-dependence degree in Reversible Hydrogen Electrode (RHE) scale:

$$\left(\frac{\partial \log j}{\partial \log [\text{OH}^-]}\right)_\eta = -\frac{\left(\frac{\partial \eta}{\partial \log [\text{OH}^-]}\right)_j}{\left(\frac{\partial \eta}{\partial \log j}\right)_{pH}} \quad (\text{S28})$$

The equation can be rearranged as below (Eq. S29 and S30), and finally the relationship of pH-dependence degree and the order of $[\text{OH}^-]/[\text{H}^+]$ is depicted as Eq. S31. The pH-dependence degree is actually a function of $[\text{OH}^-]$ and Tafel slope.

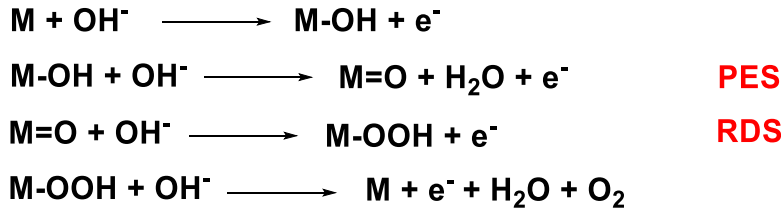
$$\left(\frac{\partial \log j}{\partial \log [\text{OH}^-]}\right)_\eta = -\frac{-\left(\frac{\partial E_{eq}}{\partial \log [\text{OH}^-]}\right)_j + \left(\frac{\partial E}{\partial \log [\text{OH}^-]}\right)_j}{\left(\frac{\partial E}{\partial \log j}\right)_{pH}} \quad (\text{S29})$$

Since *Tafel slope* = $\left(\frac{\partial \eta}{\partial \log j}\right)_{pH} = \left(\frac{\partial E}{\partial \log j}\right)_{pH}$, and the equilibrium potential of OER changed as -59 mV/dec with $[\text{OH}^-]$ (-59 mV/pH). Thus we have:

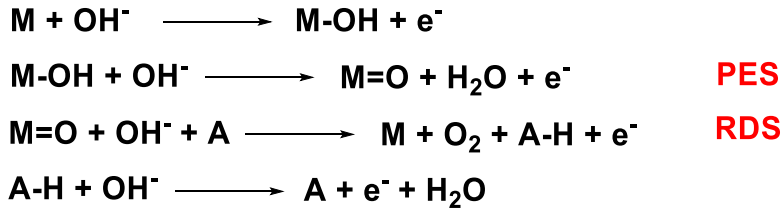
$$\left(\frac{\partial \log j}{\partial \log [\text{OH}^-]}\right)_\eta = -\frac{59 \text{ mV/dec} + \left(\frac{\partial E}{\partial \log [\text{OH}^-]}\right)_j}{\left(\frac{\partial E}{\partial \log j}\right)_{pH}} \quad (\text{S30})$$

$$\left(\frac{\partial \log j}{\partial \log [\text{OH}^-]}\right)_\eta = \left(\frac{\partial \log j}{\partial \log [\text{OH}^-]}\right)_E - \frac{59 \text{ mV/dec}}{\left(\frac{\partial E}{\partial \log j}\right)_{pH}} \quad (\text{S31})$$

1.3 Application of the kinetics model in this work



Scheme S2. General steps of traditional OER mechanisms in alkaline condition.^[10]



Scheme S3. General steps of bifunctional OER mechanisms in alkaline conditions.^[1]

For the catalysts in this work, the catalytic process involved a OH^-/e^- pre-equilibrium step followed by a OH^-/e^- rate-determining step, as mentioned in the main text. In this case $n_2 = n_4 = 1$, $m_1 = n_3 = 1$. According to Marcus theory, the transfer coefficient α is related to the driving force ΔG (overpotential) and the reorganization energy λ (Eq. S32).^[9]

$$\alpha = \frac{1}{2} \times \left(1 + \frac{\Delta G}{\lambda}\right) \quad (\text{S32})$$

When the overpotential is not high, the driving force is much smaller than the reorganization energy. Ideally the transfer coefficient is 0.5 in this case, when the diffuse double layer effects were eliminated (a concentrations of electrolyte bigger than 0.5 M is sufficient to eliminate diffuse double layer effects). The theoretical Tafel slope is $2.303RT/1.5F = 40$ mV/dec, the overall rate of the reaction is:

$$j = k^0 a_{\text{OH}^-}^2 \exp\left(\frac{3EF}{2RT}\right) \quad (\text{S33})$$

Both conventional and bifunctional OER mechanisms (Scheme S2 and S3) fit well with 40 mV/dec Tafel slope, albeit they have different RDS.

In this work, we found that the Tafel slope of bulk NiFe LDH is a little bit higher than theoretical value (40 mV/dec). The charge transfer barrier should be considered in this case. Typically, only a fraction, x ($0 < x < 1$), of the applied potential E between electrode and electrolyte is effective for interfacial electron transfer, while the other part is required to overcome the electronic resistance across the film.^[8a, 11] Therefore, the actual driving force is xE . Eq. S25 is modified as:

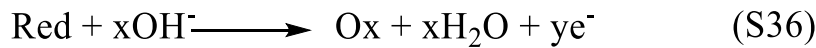
$$j = k^0 a_{\text{OH}^-}^{n_1+n_3} \exp\left(\frac{(n_2+n_4\alpha_2)xEF}{RT}\right) \quad (\text{S34})$$

The Tafel slope is now diverted as:

$$\left(\frac{\partial E}{\partial \log j}\right)_{pH} = \left(\frac{\partial \eta}{\partial \log j}\right)_{pH} = \frac{2.303RT}{(n_2+n_4\alpha_2)xF} \quad (\text{S35})$$

Hence, the Tafel slope will be increased in the presence of electronic resistance across the film. During OER catalysis, OH^- is inside the layers of LDH.^[12] Higher concentration of OH^- will alleviate electronic resistance.

In all cases, the initial step(s) should be the oxidation of the active centers accompanied with proton transfers, or the formation of M-OH (Eq. S36, Scheme S2 and S3). Such steps are typically reversible and rapid, which can be described by Nernst equation (Eq. S37). Here, x is number of protons being transferred while y is the number of electrons being transferred at the same time.



$$E = E_0 - \frac{RT}{yF} \ln\left(\frac{[\text{Red}][\text{OH}^-]^x}{[\text{Ox}]}\right) \quad (\text{S37})$$

The ratio of $[Red]/[Ox]$ is 1 at equilibrium. Therefore, Eq. S37 can be rearranged as:

$$E = E'_0 - \frac{2.303xRT}{yF} \lg([OH^-]) \quad (S38)$$

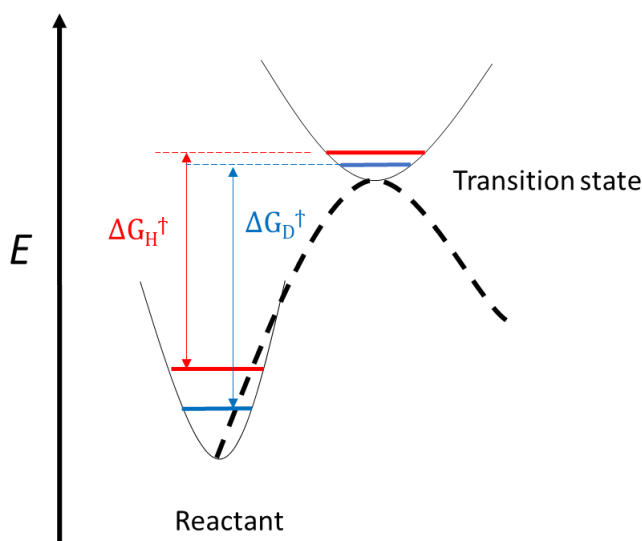
The ratio of x/y can be determined by the slope of potential - log $[OH^-]$ curves. In this study, the redox process of Ni(II)/Ni(III) was close to $3OH^-/2e^-$.

Appendix 2 H-D isotope effect

H-D isotope effect (IE) is the change of the reaction rate of a chemical reaction when one of the H atoms in the reactants is replaced by a deuterium. In electrochemical reaction, the change of the reaction rate is reflected by the variation of current density. For OER in alkaline condition, the key reactants are hydroxyl ions and adsorbed *OH and *O species. Since H of adsorbed *OH is rapidly exchanged with D, the H-D isotope effect can be investigated by measure the activity difference between KOH water solution and KOD heavy water solution (Eq. S6).

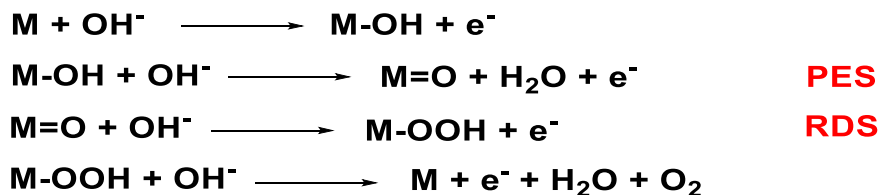
$$IE = \frac{j_{KOH}}{j_{KOD}} \quad (S5)$$

This change in reaction rate is a quantum mechanical effect. Compared to their lighter counterparts (like H), heavier isotopes (like D) will lead to lower vibration frequencies, or viewed quantum mechanically, lower zero-point energy (ZPE).^[13] With a lower ZPE, greater energetic input is required to reach the transition state, resulting in a higher activation energy for bond cleavage, consequently, a slower reaction rate (Scheme S4).^[13]

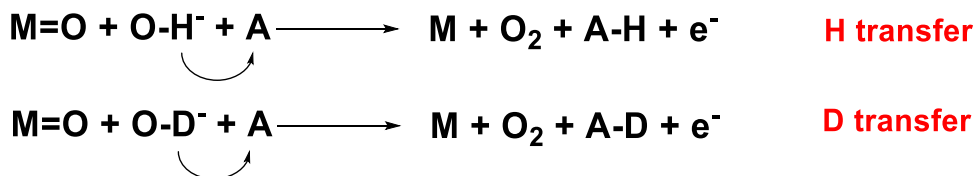


Scheme S4. Illustration of H/D isotope effect via energy diagram. ΔG_{H^\ddagger} and ΔG_{D^\ddagger} represent the activation energy of original and deuterium-substituted reactants, respectively. Typically, ΔG_{H^\ddagger} is smaller than ΔG_{D^\ddagger} .

There are two types of KIE, the primary KIE and the secondary KIE.^[6, 13] Primary KIE is found when a bond to the isotopically-labeled atom is being formed or broken. For a multi-step reaction, the observation of a primary KIE is indicative of breaking/forming a bond to the isotopically-labeled atom at the RDS.^[13] In this study, the steps indicated in Scheme S5 and S6 involve direct H/D breaking, which should exhibit primary KIE.

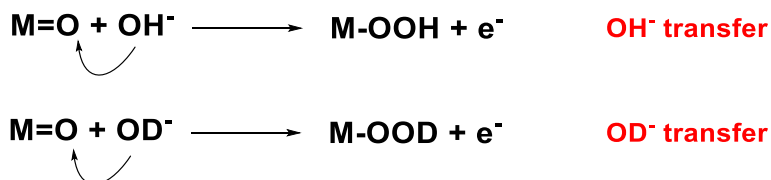


Scheme S5. The illustration of PES, which involves primary isotope effect.



Scheme S6. The illustration of RDS, which involves primary isotope effect.

Secondary KIE is observed when no bond to the isotopically-labeled atom in the reactant is broken or formed, but a neighboring bond of isotopically-labeled atom is broken or formed.^[6, 13a] Take the reactions in Scheme S7 as an example, neither direct O-H(D) break nor formation happens. Only an O-O bond close to H/D is formed. The observed isotope effect is originated from difference of ZPE between O-OH⁺ and O-OD⁺. Secondary KIEs tend to be much smaller than primary KIEs, typically in the range of 1.0-1.3.^[6, 13a]



Scheme S7. The illustration of RDS, which involved secondary isotope effect.

It should be noted that the exchange of H by D affects both the thermodynamics and the kinetics of PCET reactions.^[14] Thus, the observed isotope effect can be divided as the thermodynamic isotope effect (TIE) and the kinetic isotope effect (KIE). The TIE is originated from a change in the reaction thermodynamics or shift of the equilibria due to an increase in the vibrational ZPE of a certain bond involving hydrogen.^[14a, 15] In this study, H/D TIE effect should be observed in PES that involved proton transfer, while KIE is usually employed to determine whether proton transfer is involved in RDS.^[6, 13b, 14b] The overall isotope effect (IE) is the combination of TIE and KIE (Eq. S39).

$$IE = KIE \times TIE \quad (\text{S39})$$

In quasi Langmuir model, the reaction rate is depicted as Eq. S25 in Appendix 1, as below:

$$j = 4Fv = k^0 a_{OH^-}^{n_1+n_3} \exp\left(\frac{(n_2+n_4\alpha_2)EF}{RT}\right) \quad (S25)$$

The isotope effect should be compared in the same overpotential since the equilibrium potential is different when hydrogen is substituted by deuterium. Thus, Eq. S25 should be rearranged as below:

$$j = k_0 a_{OH^-}^{n_1+n_3} \exp\left(\frac{(n_2+n_4\alpha_2)\eta F}{RT}\right) \quad (S40)$$

$$k_0 = k^0 \exp\left(\frac{(n_2+n_4\alpha_2)E_{eq}F}{RT}\right) \quad (S41)$$

When hydrogen is substituted by deuterium, the reaction rate is changed but the reaction mechanism should remain unchanged. Thus, Eq. S40 is modified as Eq. S42:

$$j' = 4Fv' = k_0' a_{OD^-}^{n_1+n_3} \exp\left(\frac{(n_2+n_4\alpha_2')\eta F}{RT}\right) \quad (S42)$$

Considering the reaction mechanism involved in this study, the isotope effect is:

$$IE = \frac{k_0}{k_0'} \exp\left(\frac{(\alpha_2-\alpha_2')\eta F}{RT}\right) \quad (S43)$$

The expression of the rate constant k_0 and k_0' are as below:

$$k_0 = 4Fk_2^0 K_1^0 \theta_A \exp\left(\frac{(n_2+n_4\alpha_2)E_{eq}F}{RT}\right) \quad (S44)$$

$$k_0' = 4Fk_2^{0'} K_1^{0'} \theta_A' \exp\left(\frac{(n_2+n_4\alpha_2')E_{eq}F}{RT}\right) \quad (S45)$$

From the above analysis, the apparent value of isotope effect can be deconvoluted into TIE and KIE:

$$IE = KIE \times TIE = \frac{k_2^0 K_1^0 \theta_A}{k_2^{0'} K_1^{0'} \theta_A'} \exp\left(\frac{(n_2+n_4\alpha_2)(E_{eq}-E_{eq}')F}{RT}\right) \exp\left(\frac{(\alpha_2-\alpha_2')\eta F}{RT}\right) \quad (S46)$$

$$TIE = \frac{K_1^0 \theta_A}{K_1^{0'} \theta_A'} \exp\left(\frac{(n_2+n_4\alpha_2)(E_{eq}-E_{eq}')F}{RT}\right) \quad (S47)$$

$$KIE = \frac{k_2^0}{k_2^{0'}} \exp\left(\frac{(\alpha_2-\alpha_2')\eta F}{RT}\right) \quad (S48)$$

At moderate applied overpotentials, the surface concentration of key intermediate (resting state, θ_B) is less than 10%.^[8] Hence θ_A (as well as θ_A') is regarded as a potential-independent constant. The equilibrium constant K_1^0 and $K_1^{0'}$ are also potential-independent parameters, Therefore, TIE is not potential-dependent. In the case that only secondary KIE exists in RDS (for NiFe LDH in this study), the difference between α_2 and α_2' is typically small. Therefore, the observed isotope effect is dominated by TIE, which has a small change within increasing overpotentials.

According to Eq. S48, KIE is usually potential dependent. When the α_2 is bigger than α_2' , KIE increases with increasing overpotential. Vice versa when the α_2 is smaller than α_2' . Typically α_2 is bigger than α_2' due to higher barrier of charge transfer in the situation of deuterium-substitution.^[6] In the Tafel region, α_2 and α_2' are not potential-dependent, the logarithm (or ln) of KIE or overall value of isotope effect is linear dependent on overpotential. Higher overpotential results higher isotope effect value. Such results were observed for FeOOH-NiOOH, where direct hydrogen transfer was involved in RDS.

At higher overpotentials, the KIE values may deviate from this relationship due to many reasons.^[6] For examples, the transfer coefficient α_2 and α_2' become potential-dependent at high overpotentials. The change of the RDS or overall reaction mechanisms, and the variation of surface coverage of resting state will also contribute to a deviation.

In 1 M KOH(D), FeOOH-NiOOH exhibited a decrease of isotope effect with increasing overpotential at low overpotentials (below 0.22 V). At these potentials Ni(OH)₂/NiOOH are in equilibrium (Fig. 1a of maintext). The concentration of the internal hydrogen acceptor (NiOOH) may change with the applied potential, resulting a potential-dependent k_0 or k_0' .

The isotope effect of FeOOH-NiOOH is also dependent on the concentration of KOH (or pH values). This dependence might be related to the dependence of the concentration of the internal hydrogen acceptor on pH. In the literature a lower KIE was observed at a higher concentration of buffer electrolyte.^[16]

References

- [1] F. Song, M. M. Busch, B. Lassalle-Kaiser, C.-S. Hsu, E. Petkucheva, M. Bensimon, H. M. Chen, C. Corminboeuf, X. Hu, *ACS Cent. Sci.* **2019**, *5*, 558-568.
- [2] X. Xu, F. Song, X. Hu, *Nat Commun* **2016**, *7*, 12324.
- [3] L. Xu, Z. Wang, X. Chen, Z. Qu, F. Li, W. Yang, *Electrochim Acta* **2018**, *260*, 898-904.
- [4] L. Trotochaud, S. L. Young, J. K. Ranney, S. W. Boettcher, *J Am Chem Soc* **2014**, *136*, 6744-6753.
- [5] C. C. McCrory, S. Jung, J. C. Peters, T. F. Jaramillo, *J Am Chem Soc* **2013**, *135*, 16977-16987.
- [6] K. Sakaushi, *Phys Chem Chem Phys* **2020**, *22*, 11219-11243.
- [7] H. Yin, L. Jiang, P. Liu, M. Al-Mamun, Y. Wang, Y. L. Zhong, H. Yang, D. Wang, Z. Tang, H. Zhao, *Nano Research* **2018**, *11*, 3959-3971.
- [8] (a) M. E. G. Lyons, M. P. Brandon, *J Electroanal Chem* **2010**, *641*, 119-130; (b) J. O. M. Bockris, *J Chem Phys* **1956**, *24*, 817-827; (c) D. K. Bediako, Y. Surendranath, D. G. Nocera, *J Am Chem Soc* **2013**, *135*, 3662-3674.
- [9] A. J. Bard, L. R. Faulkner, J. Leddy, C. G. Zoski, *Electrochemical methods: fundamentals and applications*, Vol. 2, Wiley New York, **1980**.
- [10] I. C. Man, H.-Y. Su, F. Calle-Vallejo, H. A. Hansen, J. I. Martínez, N. G. Inoglu, J. Kitchin, T. F. Jaramillo, J. K. Nørskov, J. Rossmeisl, *ChemCatChem* **2011**, *3*, 1159-1165.
- [11] (a) D. Y. Chung, S. Park, P. P. Lopes, V. R. Stamenkovic, Y.-E. Sung, N. M. Markovic, D. Strmcnik, *ACS Catal* **2020**, *10*, 4990-4996; (b) H. Vrubel, T. Moehl, M. Gratzel, X. Hu, *Chem Commun* **2013**, *49*, 8985-8987.
- [12] R. Chen, S. F. Hung, D. Zhou, J. Gao, C. Yang, H. Tao, H. B. Yang, L. Zhang, L. Zhang, Q. Xiong, H. M. Chen, B. Liu, *Adv Mater* **2019**, *31*, e1903909.
- [13] (a) M. Gómez-Gallego, M. A. Sierra, *Chem Rev* **2011**, *111*, 4857-4963; (b) L. I. Krishtalik, *Electrochim Acta* **2001**, *46*, 2949-2960.
- [14] (a) G. Parkin, *Acc Chem Res* **2009**, *42*, 315-325; (b) W. Zhang, I. J. Burgess, *J Electroanal Chem* **2012**, *668*, 66-72.
- [15] C. Pasquini, I. Zaharieva, D. Gonzalez-Flores, P. Chernev, M. R. Mohammadi, L. Guidoni, R. D. L. Smith, H. Dau, *J Am Chem Soc* **2019**, *141*, 2938-2948.
- [16] (a) Y. Zhang, H. Zhang, H. Ji, W. Ma, C. Chen, J. Zhao, *J Am Chem Soc* **2016**, *138*, 2705-2711; (b) W. Li, F. Li, H. Yang, X. Wu, P. Zhang, Y. Shan, L. Sun, *Nat Commun* **2019**, *10*, 5074.